Mon. Not. R. Astron. Soc. **362,** 424–454 (2005) doi:10.1111/j.1365-2966.2005.09325.x

The abundance discrepancy – recombination line versus forbidden line abundances for a northern sample of galactic planetary nebulae

R. Wesson,[1] X-W. Liu[1,2] and M. J. Barlow[1]★

[1]*Department of Physics and Astronomy, University College London, Gower Street, London WC1E 6BT*

[2]*Department of Astronomy, Peking University, Beijing 100871, China*

Accepted 2005 June 2. Received 2005 May 20; in original form 2004 August 18

ABSTRACT

We present deep optical spectra of 23 galactic planetary nebulae, which are analysed in conjunction with archival infrared and ultraviolet spectra. We derive nebular electron temperatures based on standard collisionally excited line (CEL) diagnostics as well as the hydrogen Balmer jump and find that, as expected, the Balmer jump almost always yields a lower temperature than the [O III] nebular-to-auroral line ratio. We also make use of the weak temperature dependence of helium and O II recombination line ratios to further investigate the temperature structure of the sample nebulae. We find that, in almost every case, the derived temperatures follow the relation T_e(CEL) $\geqslant$ T_e(BJ) $\geqslant$ T_e(He I) $\geqslant$ T_e(O II), which is the relation predicted by two-component nebular models in which one component is cold and hydrogen-deficient. T_e(O II) may be as low as a few hundred Kelvin, in line with the low temperatures found for the hydrogen-deficient knots of Abell 30 by Wesson, Liu and Barlow.

Elemental abundances are derived for the sample nebulae from both CELs and optical recombination lines (ORLs). ORL abundances are higher than CEL abundances in every case, by factors ranging from 1.5 to 12. Five objects with O^{2+} abundance discrepancy factors greater than 5 are found. DdDm 1 and Vy 2–2 are both found to have a very large abundance discrepancy factor of 11.8.

We consider the possible explanations for the observed discrepancies. From the observed differences between T_e(O III) and T_e(BJ), we find that temperature fluctuations cannot resolve the abundance discrepancies in 22 of the 23 sample nebulae, implying some additional mechanism for enhancing ORL emission. In the one ambiguous case, the good agreement between abundances derived from temperature-insensitive infrared lines and temperature-sensitive optical lines also points away from temperature fluctuations being present. The observed recombination line temperatures, the large abundance discrepancies and the generally good agreement between infrared and optical CEL abundances all suggest instead the existence of a cold hydrogen-deficient component within the 'normal' nebular gas. The origin of this component is as yet unknown.

Key words: ISM: abundances – planetary nebulae: general.

1 INTRODUCTION

A long-standing problem in nebular astrophysics is that abundances derived from optical recombination lines (ORLs) are universally higher than those derived from collisionally excited lines (CELs). The discrepancies observed are typically a factor of 2–3, but exceed a factor of 5 in approximately 5 per cent of planetary nebulae. The most extreme cases known are NGC 1501, Hf 2–2 and Abell 30, for which the abundance discrepancies for O^{2+} are factors of 32, 84 and 700, respectively (Liu 2003; Wesson et al. 2003; Ercolano et al. 2004). Closely linked to this problem is the discrepancy whereby electron temperatures derived from the hydrogen Balmer jump are systematically lower than those derived from [O III] forbidden lines.

Many theories have been advanced to resolve these discrepancies. Peimbert (1967) showed that in a thermally inhomogeneous nebula, CEL emission would be weighted towards the hotter regions, while recombination line emission would be weighted towards cooler regions. The temperatures derived from CEL diagnostics would be overestimated, and so CEL abundances would be underestimated. In this case, ORL abundances should be more reliable than CEL abundances.

★E-mail: mjb@star.ucl.ac.uk

However, while this scenario can potentially resolve small discrepancies, up to a factor of 3 or so, the discovery in recent years of more extreme objects such as NGC 7009 (Liu et al. 1995), NGC 6153 (Liu et al. 2000), M 1–42 and M2–36 (Liu et al. 2001), with discrepancies exceeding a factor of 5, has shown that temperature fluctuations cannot be the sole cause of the abundance discrepancies in the more extreme cases. Even in nebulae with more moderate discrepancies such as NGC 6543, detailed analysis by Wesson & Liu (2004) showed that the temperature fluctuations present were too small to resolve the ORL/CEL abundance discrepancy factor (adf) of 3.

Infrared (IR) fine structure lines have low excitation temperatures ($\leqslant$1000 K) compared to typical nebular temperatures, and so should be insensitive to temperature fluctuations. Therefore, if temperature fluctuations were the cause of the discrepancy, the IR lines would be expected to yield similar abundances to ORLs. However, this is shown not to be the case for many nebulae (Liu et al. 2000, 2001; Tsamis 2002; Tsamis et al. 2004).

Instead, hydrogen-deficient material present in nebulae seems to offer a more viable explanation of the observed temperature and abundance discrepancies (Liu et al. 2000; Péquignot et al. 2003). Such material would be strongly cooled by IR emission from heavy element ions, and thus CEL emission would be strongly suppressed, while ORL emission would be enhanced due to the inverse power-law temperature dependence of ORL emissivities. In this case, abundances derived from CELs would be close to the average abundance of the whole nebula, as the hot component would contain the majority of the nebular material, while ORL abundances would apply to the cold H-deficient knots. Wesson et al. (2003) showed that very cold ionized material exists in the known H-deficient knots of Abell 30, with subsequent photoionization modelling by Ercolano et al. (2003) further demonstrating the physical plausibility of the existence of ionized material at temperatures of <2000 K.

In this paper we present observations and analysis of new optical and archival IR and ultraviolet spectra of a sample of 23 planetary nebulae. Physical conditions are determined from standard forbidden diagnostics, as well as from the hydrogen recombination spectrum and recombination lines of heavy elements. Abundances are determined from both CELs and ORLs. It is shown that discrepancies between ORL and CEL abundances are present in all nebulae analysed, with values of adf(O^{2+}) [$= (O^{2+}/H^+)_{ORL}/(O^{2+}/H^+)_{CEL}$] ranging from 1.5 to 12. Possible explanations for the discrepancy are considered, and it is shown that, in almost every case, temperature fluctuations described by the formalism of Peimbert (1967) are unable to resolve the observed abundance discrepancies. Instead, there is strong evidence to suggest that cold H-deficient regions are present in most if not all planetary nebulae.

2 OBSERVATIONS

2.1 Optical spectra

The optical spectra for the planetary nebulae analysed in this section were obtained using the Intermediate Dispersion Spectrograph (IDS) on the 2.5-m Isaac Newton Telescope at the Observatorio del Roque de los Muchachos, on La Palma, Spain, between 2001 August 1 and 5. Spectra were taken covering two wavelength ranges. The R1200B grating was used to cover the range 3500–5000 Å at a resolution of 0.95 Å FWHM, thus covering most important ORLs of C^{2+}, C^{3+}, N^{2+}, N^{3+}, O^{2+} and Ne^{2+}, as well as the hydrogen Balmer jump, at high spectral resolution. The R300V grating, in conjunction with a GG385 order-sorting filter, was used to cover wavelengths from 3800–7700 Å at a resolution of 4.0 Å FWHM. These low-resolution spectra were used to derive the logarithmic extinction at Hβ, c(Hβ), from the observed ratio of Hα/Hβ, and temperatures and densities from forbidden line diagnostics. A slit 1 arcsec wide and 4 arcmin long was used for all observations. A log of the observations is given in Table 1. This table also contains published total Hβ fluxes from Cahn, Kaler & Stanghellini (1992), angular dimensions of the nebulae from the Strasbourg–European Southern Observatory (ESO) Catalogue (Acker et al. 1992) and the values of c(Hβ) derived in Section 3.1.

Table 1. Log of INT/IDS observations 2001 August 1–5.

Nebula	log F(Hβ) (erg cm^{-2} s^{-1})	Ang. diam. (arcsec)	c(Hβ)	PA (deg)	Exposures Blue (s)	Red (s)
Cn 3–1	−10.94	4.5	0.456	0	2 × 1200	300
DdDm 1	−11.57	0.6	0.137	0	1800	300
Hu 1–1	−11.60	5.0	0.554	15	1200	300
Hu 2–1	−10.80	2.6	0.777	0	1200	300
IC 1747	−11.49	13.0	1.000	0	1800	300
IC 2003	−11.19	8.6	0.347	0	2 × 1200	300
IC 351	−11.42	7.0	0.384	0	1200	300
IC 4846	−11.34	2.0	0.698	0	2 × 1200	300
IC 5217	−11.17	6.6	0.501	0	2 × 1800	300
M 1–73	−11.70	5.0	1.142	0	2 × 1800	300
M 1–74	−11.75	5.0	1.115	0	2 × 1200 2 × 1800	300
M 3–27	−11.83	1.0		0	2 × 1800	
M 3–34	−11.80	5.6	0.582	90	1800	300
Me 2–2	−11.16	5.0	0.343	0	2 × 1800	600
NGC 6803	−11.18	5.5	0.869	0	2 × 1800	600
NGC 6807	−11.48	2.0	0.642	0	1800	300
NGC 6833	−11.25	2.0	0.000	90	2 × 1800	300
NGC 6879	−11.58	5.0	0.401	90	1800	300
NGC 6891	−10.65	15.0	0.287	10	2 × 1200	300
NGC 7026	−10.90	20.0	1.115	90	1800	300
Sp 4–1	−11.84	0.0	0.000	0	2 × 1200	300
Vy 1–2	−11.53	4.6	0.139	0	2 × 1200	300
Vy 2–2	−11.56	0.5	1.653	0	2 × 1200	300

2.1.1 Data reduction

The two-dimensional image frames were reduced using the LONG92 package within MIDAS, and also IRAF. Using MIDAS, they were bias-subtracted, flat-fielded, cleaned of cosmic rays and wavelength calibrated using a Cu–Ar calibration lamp. The spectra were flux calibrated using wide-slit (6 arcsec) observations of the standard stars Feige 110, HZ 44 and BD+28 4211. IRAF was used to fit the observed flux distributions with high-order spline functions.

In all cases, the angular diameter of the nebula was less than our slit length and so suitable sky windows could be selected on either side of the nebular emission. The sky background was fitted in the direction of the slit by a second-order polynomial and subtracted from the two-dimensional image frame. Atmospheric extinction was corrected for using the published mean atmospheric extinction curve for La Palma (King 1985). Nebular emission was then summed over the observed spatial extent along the slit of the Hβ line, and the resulting one-dimensional spectra were normalized such that $F(\mathrm{H}\beta) = 100$. Multiple spectra were combined, weighted by exposure time.

Some example spectra are shown in Figs 1, 2 and 3.

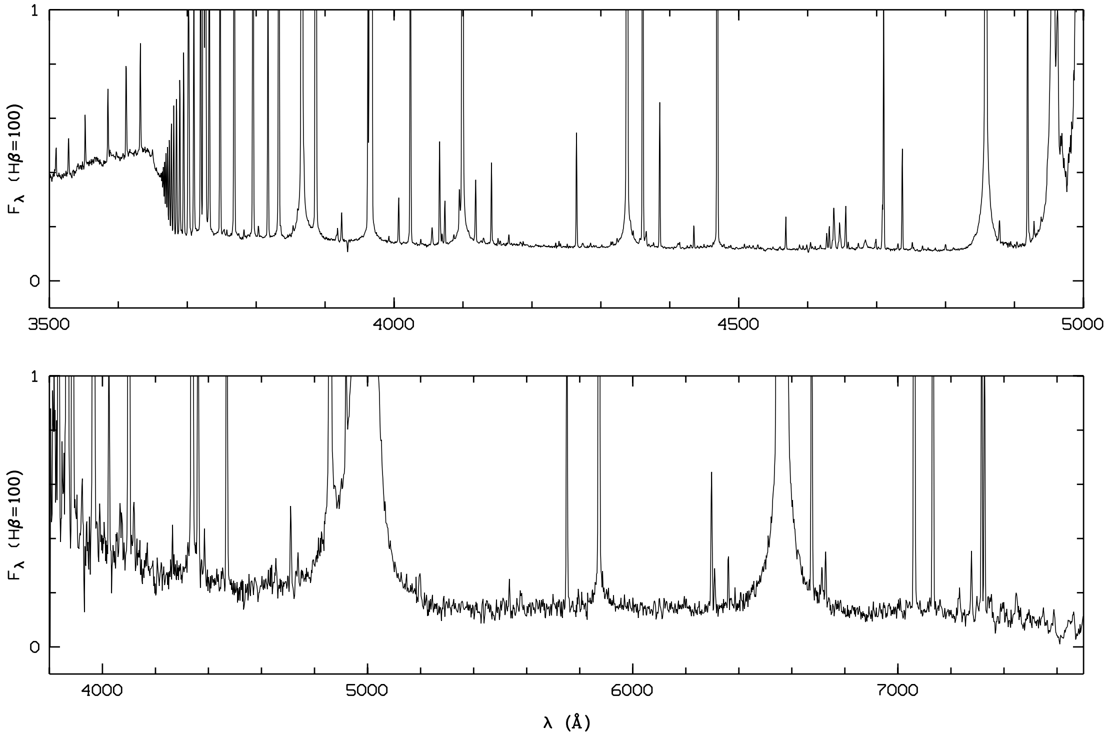

Figure 1. INT spectra of Me 2–2: grating R1200B (top) covers wavelengths of 3500–5000 Å and R300V (bottom) covers 3800–7700 Å.

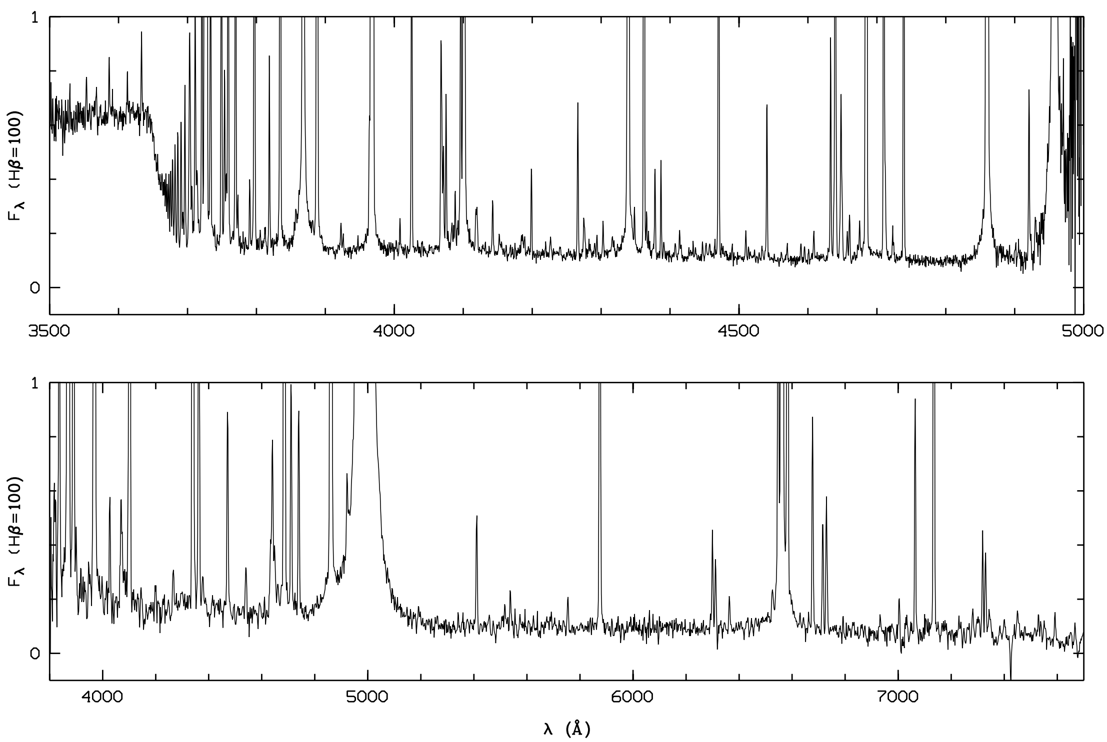

Figure 2. INT spectra of Vy 1–2: grating R1200B (top) covers wavelengths of 3500–5000 Å and R300V (bottom) covers 3800–7700 Å. Note the strong recombination lines seen in this object, particularly the C III/O II blend at 4650 Å.

2.2 *International Ultraviolet Explorer* observations

13 nebulae in this sample were observed using the *International Ultraviolet Explorer* (*IUE*) satellite. Low-resolution spectra taken with the Short Wavelength Prime (SWP) and Long Wavelength Prime (LWP) cameras were downloaded from the archive at the Space Telescope Science Institute (STScI), in their final calibrated form. Details of the observations used are given in Table 2. Where several spectra were available, those with the best signal-to-noise

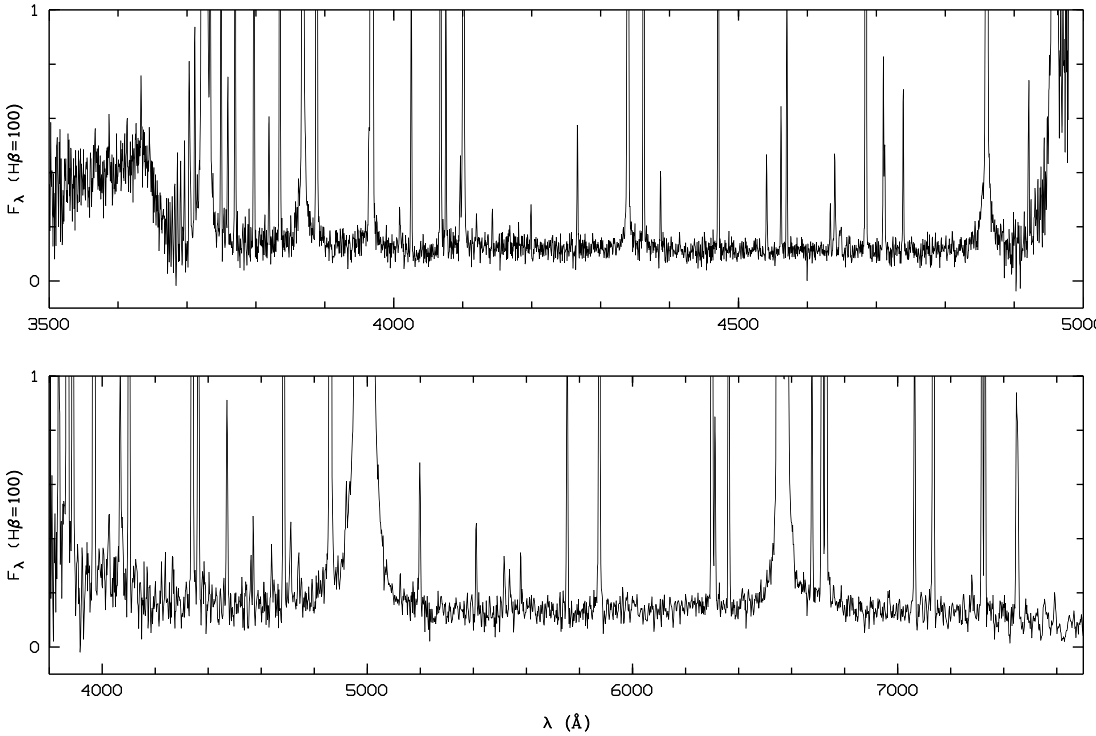

Figure 3. INT spectra of Hu 2–1: grating R1200B (top) covers wavelengths of 3500–5000 Å and R300V (bottom) covers 3800–7700 Å.

ratio were selected and combined, weighted by exposure time. For all nebulae, the angular extent of the nebula was smaller than the *IUE* large aperture (10 × 20 arcsec^2) and so all the nebular flux should have been caught. The measured fluxes were normalized to H$\beta = 100$ using the total Hβ fluxes listed by Cahn et al. (1992), and dereddened using the extinction coefficients derived from the optical spectra.

Table 2. *IUE* observations of the sample nebulae.

Nebula	SWP		LWR/LWP	
	Exposure	Exposure time (s)	Exposure	Exposure time (s)
DdDm 1	23840	6720	04145	9000
	23872	3600	18711	3600
	39590	8100		
Hu 2–1	06642	1200	05703	2400
	08589	2400		
IC 1747	35633	3600	15112	3600
	35634	10 200		
IC 2003	07260	1800	06255	2700
	07261	5400		
IC 351	21158	7200	08206	2700
IC 4846	33381	3600	13130	4800
IC 5217	06257	1440	01785	2400
	07257	4320	05429	2160
M 1–74	30975	1800	10769	1567
M 3–27	22700	7200	03259	2700
NGC 6803	06256	3600	05428	3600
NGC 6833	31708	3600		
	31826	1800		
NGC 6891	44984	1200		
NGC 7026	51698	10 800	28800	10 800
Vy 1–2	33542	2700	13245	2700
	33543	8100		

2.3 *Infrared Space Observatory* observations

Four nebulae in the sample (Hu 2–1, Me 2–2, NGC 6891 and Vy 2–2) were observed with the *Infrared Space Observatory (ISO)* Short Wavelength Spectrometer (SWS), and the fully calibrated spectra were downloaded from the *ISO* archive. The *ISO* SWS aperture depends on wavelength, being 14 × 20 arcsec^2 for wavelengths of 2.38–12 μm, 14 × 27 arcsec^2 for wavelengths of 12–27.5 μm, 20 × 27 arcsec^2 for wavelengths of 27.5–29 μm and 20 × 33 arcsec^2 for wavelengths of 29–45 μm. These apertures are all larger than the angular dimensions of the nebulae observed, and so the measured fluxes were simply normalized to $F(\mathrm{H}\beta) = 100$ using published total Hβ fluxes from Cahn et al. (1992). The fluxes were then dereddened using the values of $c(\mathrm{H}\beta)$ derived from the optical spectra and the galactic extinction law of Howarth (1983).

2.4 Data analysis

The fluxes of lines in the optical and UV spectra were measured using Gaussian line profile fitting techniques within MIDAS. The weak ORLs are often subject to line blending, even at the high resolution of the blue spectra. For example, four lines of the O II V10 multiplet are blended with two [S II] lines in the 4068–4076 Å wavelength range, and three C III V1 and two O II V1 lines are usually seen to form a single broad feature around 4650 Å. In such cases, line fluxes were measured by fitting multiple Gaussians. To obtain a good line fit, it was sometimes necessary to constrain the linewidths to have the same FWHM as a nearby unblended line. In cases where a satisfactory fit was still difficult to obtain, the relative fluxes of recombination lines from the same multiplet were fixed assuming LS coupling; for example, in the case of the 4650 O II/C III feature, the three C III lines at 4647.42, 4650.25 and 4651.47 Å are predicted to have strengths in the ratio 5 : 3 : 1. Examples of Gaussian profile fits to blended lines are shown in Fig. 4.

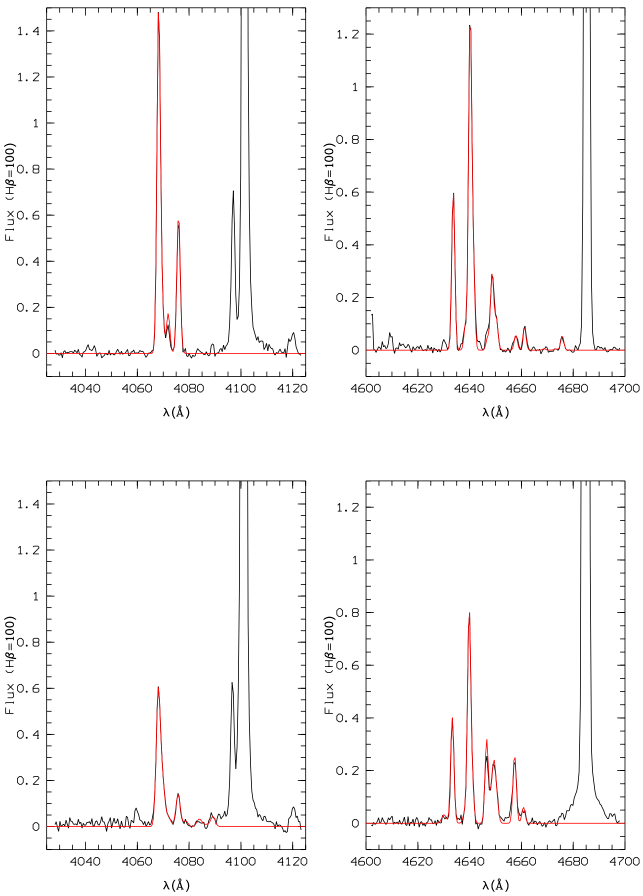

Figure 4. Examples of line deblending in IC 2003 (top) and NGC 7026 (bottom): the O II/[S II] blend at 4068–4076 Å and the O II/C III blend at 4650 Å.

A full list of the fluxes of all lines measured in the UV, optical and IR spectra for the sample nebulae is given in the Appendices.

3 NEBULAR ANALYSIS

3.1 Interstellar reddening

Before proceeding with the nebular analysis it was necessary to correct the spectra for the effects of interstellar extinction. The logarithmic extinction at Hβ, $c(\mathrm{H}\beta)$, was determined by comparing the observed Hα/Hβ ratio to the value of 2.85 predicted by Storey & Hummer (1995) for $T_{\mathrm{e}} = 10\,000$ K and $N_{\mathrm{e}} = 5\,000$ cm^{-3}, reasonable first guesses for planetary nebulae. All line intensities were then dereddened using the formula

$$I(\lambda) = 10^{c(\mathrm{H}\beta)f(\lambda)} F(\lambda), \tag{1}$$

where $f(\lambda)$ describes an appropriate interstellar extinction curve. We adopt the galactic reddening law of Howarth (1983). The derived values of $c(\mathrm{H}\beta)$ for the sample nebula are given in Table 1. In the case of M 3–27, for which only blue spectra were available, $c(\mathrm{H}\beta) = 0.98$ was taken from Tylenda et al. (1992).

3.2 Physical conditions

For all nebulae in the sample except M 3–27, which is discussed below, temperatures were derived from the [O III] $\lambda\lambda$4959+5007/λ4363 forbidden line ratio. Temperatures were also derived from the ratios [N II] $\lambda\lambda$6548+6584/λ5755, [O II] $\lambda\lambda$7320+7330/λ3727 and [S II] $\lambda\lambda$6731+6717/λ4068, for the nebulae where the relevant lines were all detected. The density derived from the [O II] λ3727/3729 ratio was adopted for all temperature derivations. Temperatures were also derived in all cases from the ratio of the hydrogen Balmer jump to H11, using the following equation given by Liu et al. (2001)

$$T_{\mathrm{e}} = 368(1 + 0.259y^{+} + 3.409y^{++})\left(\frac{\mathrm{BJ}}{\mathrm{H11}}\right)^{-(3/2)}, \tag{2}$$

where $y^{+} = \mathrm{He}^{+}/\mathrm{H}^{+}$, $y^{++} = \mathrm{He}^{++}/\mathrm{H}^{+}$, and BJ/H11 is in units of Å^{-1}. Two examples of spectra in the region of the Balmer jump are shown in Fig. 5.

Densities were derived from the forbidden line ratios [Ar IV] λ4711/λ4740, [Cl III] λ5517/λ5537, [S II] λ6716/λ6731 and [O II] λ3727/λ3729. [O II] densities were derived for all nebulae in the sample. In the case of other density diagnostics, the lines were not always visible.

The derived electron temperature and density diagnostics are presented in Tables 3 and 4, respectively. Fig. 6 shows the Balmer jump temperature plotted against the [O III] temperature, and clearly shows that, in almost every case, the Balmer jump temperature is lower than the [O III] temperature. While T_{e}([O III]) always lies between 7500 and 13 000 K, the Balmer jump temperatures cover a larger range of values, from as low as 5000 K to almost 14 000 K. Also plotted in Fig. 6 are lines showing the relation between T_{e}(BJ) and T_{e}([O III]) for several values of t^2, the temperature fluctuation parameter defined by Peimbert (1967).

These results are in line with the results of Liu & Danziger (1993), who measured T_{e}([O III]) and T_{e}(BJ) for 14 nebulae. They found that a temperature difference corresponding to $t^2 = 0.03$ was typical for their sample. The average value measured for the current sample is higher at $\sim$0.05.

While the differences observed between T_{e}(BJ) and T_{e}([O III]) can theoretically be accounted for by temperature fluctuations within a chemically homogeneous gas (Peimbert 1967), there are some significant difficulties with this interpretation, as outlined in the introduction. In Sections 4.3.3 and 4.4.4, temperatures derived from other recombination line diagnostics are used to shed further light on the temperature structure of the sample nebulae, and evidence against the actual existence of substantial temperature fluctuations is further discussed in Section 6.2.

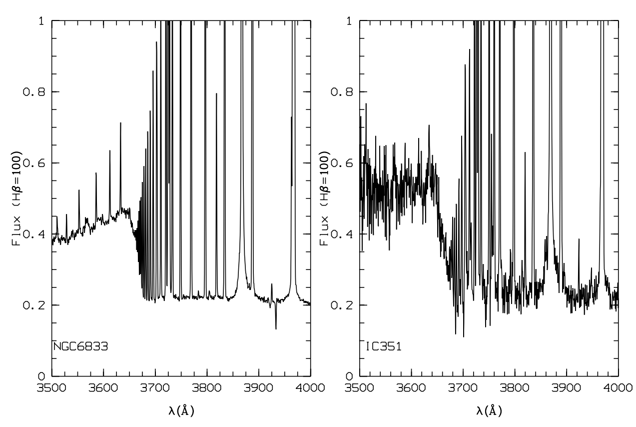

Figure 5. Spectra of NGC 6833 and IC 351 in the region of the hydrogen Balmer jump at 3646 Å.

Table 3. Electron temperatures in K derived for the sample planetary nebulae.

Nebula	T_e([O III])	T_e([N II])	T_e([O II])	T_e([S II])	T_e(BJ)
Cn 3–1	7670	7840	7520	6300	5090
DdDm 1	12 300	12 980	16 110	13 850	8730
Hu 1–1	12 110	11 160	*	8850	8350
Hu 2–1	9860	12 340	16 030	*	8960
IC 1747	10 850	12 100	10 880	12 320	9650
IC 2003	12 650	13 430	15 640	16 250	8960
IC 351	13 070	*	*	2530	11 050
IC 4846	10 710	*	10 610	6720	7700
IC 5217	11 270	*	*	*	11 350
M 1–73	7450	8660	7260	7410	5490
M 1–74	10 150	12 200	8250	7120	7850
M 3–27	13 000	*	*	*	9020
M 3–34	12 230	*	*	*	8440
Me 2–2	10 970	13 270	*	*	10 590
NGC 6803	9740	11 080	17 680	8205	7320
NGC 6807	10 930	16 050	*	13 730	9900
NGC 6833	12 810	*	*	*	13 670
NGC 6879	10 400	*	*	*	8500
NGC 6891	9330	*	*	*	5930
NGC 7026	9310	10 080	14 720	10 350	7440
Sp 4–1	11 240	16 240	*	*	8830
Vy 1–2	10 400	*	16 179	*	6630
Vy 2–2	13 910	*	*	*	9300

Table 4. Electron densities in cm^{-3} derived for the sample planetary nebulae.

Object	N_e([O II])	N_e([S II])	N_e([Cl III])	N_e([Ar IV])	Mean
Cn 3–1	4130	9480	6890	*	6830
DdDm 1	4000	*	*	5000	4500
Hu 1–1	1250	1380	*	1460	1360
Hu 2–1	7870	*	*	*	7870
IC 1747	2630	3930	*	2400	2980
IC 2003	2710	5180	2050	2590	3130
IC 351	1740	3570	*	2600	2630
IC 4846	5460	20 210	*	7230	10 960
IC 5217	5090	*	6240	2220	4510
M 1–73	2860	6130	*	*	4490
M 1–74	6900	46 630	*	18 560	24 030
M 3–27	3220	*	*	*	3220
M 3–34	4010	*	*	2990	3500
Me 2–2	10 800	2000	*	23 000	11 930
NGC 6803	4070	7450	*	10 050	7190
NGC 6807	7770	13 850	*	33 970	18 530
NGC 6833	19 030	*	*	*	19 030
NGC 6879	4450	*	*	4320	4380
NGC 6891	1760	*	*	1560	1660
NGC 7026	2710	*	8060	5770	5510
Sp 4–1	1880	*	*	*	1880
Vy 1–2	4100	1160	*	3300	2850
Vy 2–2	20 530	11 730	*	*	16 130

3.2.1 M 3–27

M 3–27 is thought to be an extremely dense, young object (e.g. Kohoutek 1968; Barker 1978). The [O II] λ3727/λ3729 line ratio implies a fairly low density of 3220 cm^{-3}, but the unusually large [O III] λ4363/λ4959 intensity ratio is only possible if the density is very high. To determine the physical conditions in this object, we first made use of the sensitivity of high-order hydrogen Balmer lines to density. Fig. 7 shows the observed intensities of the high-order hydrogen Balmer lines in M 3–27, together with theoretical intensities at varying densities from Storey & Hummer (1995). The observed intensities are consistent with an electron density of 10^7 cm^{-3}. Adopting this density, the observed [O III] λ4959/λ4363 ratio yields a temperature of 13 000 K.

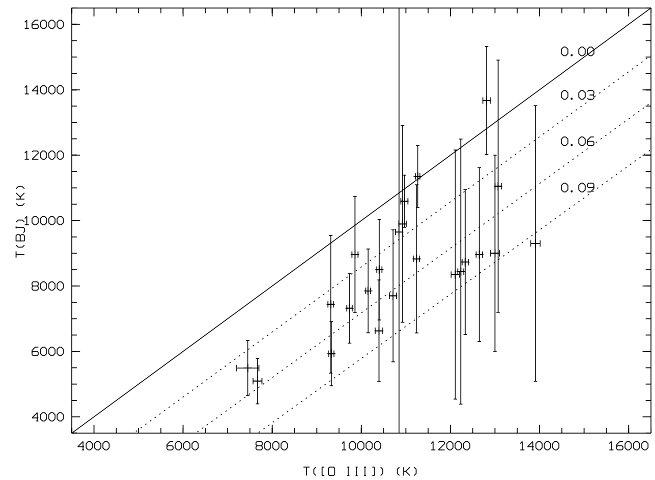

Figure 6. Balmer jump versus [O III] temperatures. The lines show the relation between the measured T_e(BJ) and T_e([O III]) for different values of the temperature fluctuation parameter t^2 (see text).

Subsequent abundance analysis shows that adopting this extremely high density yields a very high O^+/H^+ abundance, larger than the O^{2+}/H^+ abundance. This would imply a nebula of very low excitation, in contradiction with the observations of higher ionization stages such as Ar^{3+} and the very strong [O III] λ4363 emission. Adopting the lower density implied by the [O II] λ3727/λ3729 ratio to derive the O^+/H^+ abundance yields a much lower and more plausible value. It seems likely that emission from doubly and more highly ionized species comes predominantly from the very dense core of the nebula, while emission from singly ionized species arises in a lower density outer region. The planetary nebulae Mz 3 (Zhang & Liu 2002) and M2–24 (Zhang & Liu 2003) show very similar behaviour, with high ionization species existing predominantly in a dense central core.

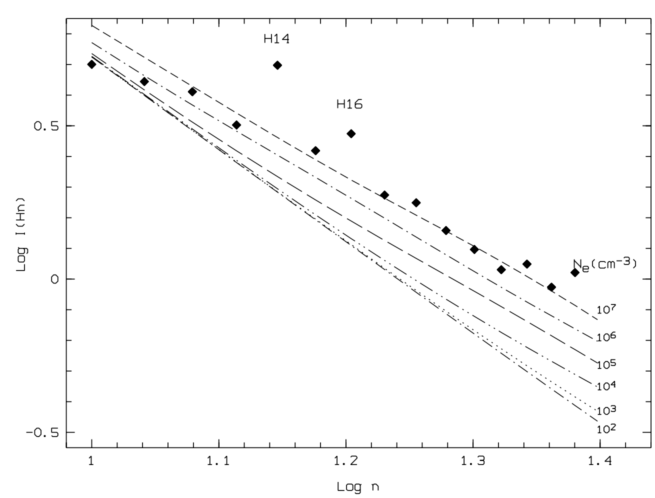

Figure 7. High-order hydrogen Balmer line intensities in M 3–27; note that H14 and H16 are affected by blending.

In subsequent abundance determinations, $T_e = 13\,000$ K is adopted for all species, with $N_e = 3220$ cm^{-3} being adopted for singly ionized species and $N_e = 10^7$ cm^{-3} being adopted for all higher ionization stages.

3.2.2 Recombination excitation of N II and O II auroral lines

The agreement between the various temperature diagnostics is not always very good. The average T_e([O III]) for the whole sample is 11 290 K, while the average T_e([N II]) is 13 350 K. For the 13 nebulae for which both temperatures are measured, the averages are 10 400 and 12 110 K, respectively. For T_e([O III]) and T_e([O II]), for the 11 nebulae in which both temperatures are measured, the averages are 10 100 and 12 800 K. The generally higher temperatures measured for singly ionized species than those for doubly ionized species have sometimes been interpreted as due to the hardening of the radiation field in the less-ionized outer regions of planetary nebulae. However, a more likely explanation is that the lower efficiencies of the [O II] and [N II] cooling lines, compared to those of [O III], leads to higher electron temperatures in outer nebular regions where singly ionized elements dominate.

Given that generally most of the N and O is in the form of N^{2+} and O^{2+}, recombination of the doubly ionized ions can contribute significantly to the flux in the [N II] and [O II] nebular and auroral lines (Rubin 1986). Liu et al. (2000) calculated radiative and dielectronic recombination coefficients for the metastable levels of [O II], and also used radiative recombination coefficients from Péquignot, Petitjean & Boisson (1991) and dielectronic recombination coefficients from Nussbaumer & Storey (1984) for [N II] to derive the following formulae for the recombination contributions to the intensities of the [N II] and [O II] auroral lines:

$$\frac{I_R(\lambda 5754)}{I(\mathrm{H}\beta)} = 3.19 t^{0.30} \frac{\mathrm{N}^{2+}}{\mathrm{H}^+}, \quad (3)$$

$$\frac{I_R(\lambda 7320 + \lambda 7330)}{I(\mathrm{H}\beta)} = 9.36 t^{0.44} \frac{\mathrm{O}^{2+}}{\mathrm{H}^+}. \quad (4)$$

Here, $t = T_e/10^4$. We used these formulae to correct the temperatures derived from the [N II] and [O II] nebular-to-auroral line ratios for the effects of recombination, using $t = T_e([\mathrm{O\,III}])/10^4$. The revised temperatures are given in Table 5. We used abundances derived from both CELs and ORLs (see Section 4), and in many cases the recombination contribution is considerable. In Table 5, the three columns listed for each of T_e([N II]) and T_e([O II]) are, from left to right, the uncorrected temperature, the temperature corrected for recombination using the CEL ionic abundance, and the temperature corrected using the ORL ionic abundance. In three cases, if the abundances derived from ORLs are used, recombination can account for the entire flux of the auroral lines (DdDm 1 and Sp 4–1 for the [N II] lines and Vy 2–2 for the [O II] lines), in which case the line ratios are no longer a useful temperature diagnostic. Accounting for recombination excitation brings the temperatures into somewhat better agreement in many cases.

Recombination excitation may also enhance the [S II] λ4068 and λ4076 lines, which are also blended with lines from the O II V10 multiplet. However, adequate accounting for the effects of recombination on these lines is hampered by the lack of effective recombination coefficients for the [S II] metastable levels. Given the blending of these lines and the possible effects of recombination excitation, the [S II] temperatures may be subject to considerable errors.

3.3 Temperatures from helium emission-line ratios

Table 3 shows that in almost every case, the electron temperature derived from the hydrogen Balmer jump is lower than that derived from the [O III] forbidden lines. This phenomenon was first observed

Table 5. Corrected electron temperatures (in K), accounting for recombination excitation of the nebular and auroral lines.

Object	T_e([O III])	T_e([N II]) Uncorrected	T_e([N II]) CEL	T_e([N II]) ORL	T_e([O II]) Uncorrected	T_e([O II]) CEL	T_e([O II]) ORL
Cn 3–1	7670	7840	*	*	7520	7520	7520
DdDm 1	12 300	12 980	*	All Rec	16 110	16 110	16 110
Hu 1–1	12 110	11 160	*	*	*	*	*
Hu 2–1	9860	12 340	*	11 520	16 030	16 520	17 140
IC 1747	10 850	12 100	11 890	*	10 880	10 430	*
IC 2003	12 650	13 430	13 360	11 280	15 640	15 640	14 810
IC 351	13 070	*	*	*	*	*	*
IC 4846	10 710	*	*	*	10 610	10 490	10 350
IC 5217	11 270	*	*	*	*	*	*
M 1–73	7450	8660	*	6570	7260	6960	6590
M 1–74	10 150	12 200	*	*	8250	8290	8630
Me 2–2	10 970	13 270	*	13 040	*	*	*
NGC 6803	9740	11 080	10 940	10 640	17 680	18 310	*
NGC 6807	10 930	16 050	*	10 930	*	*	*
NGC 6833	12 810	*	*	*	*	*	*
NGC 7026	9310	10 080	*	9670	14 720	14 860	13 870
Sp 4–1	11 240	16 240	*	All Rec	*	*	*
Vy 1–2	10 400	*	*	*	16 170	17 110	10 620
Vy 2–2	13 910	*	*	*	*	*	All Rec
Averages	10 920	12 110	12 060	10 520	13 160	11 470	9950

by Peimbert (1971), and interpreted by him and many subsequent investigators as evidence for substantial temperature fluctuations in the nebulae. The emissivity of the hydrogen continuum has a negative power-law dependence on T_e, while the emissivities of the [O II] lines increase exponentially with temperature. Thus, in the presence of temperature fluctuations, the CEL emission will be strongly weighted towards the hottest regions of the nebula, while the hydrogen continuum emission will be weighted towards the cooler regions.

A problem with the temperature fluctuation scenario is that in many cases the magnitude of the fluctuations required to reconcile T_e([O III]) and T_e(BJ) is larger than anything predicted by photoionization modelling. Alternative explanations for the observed temperature discrepancies have included the presence of strong density inhomogeneities (Viegas & Clegg 1994), extra heating from shock waves (Peimbert, Sarmiento & Fierro 1991) and abundance discontinuities (Torres-Peimbert, Peimbert & Peña 1990). Direct observational evidence for these mechanisms is lacking, however. Liu et al. (2000) proposed that the presence of cold hydrogen-deficient knots within the main body of the nebula could resolve the temperature discrepancies. In this case, CEL emission would come almost entirely from the hot, normal component of the nebula, with most of the ORL emission originating from the cold knots. Helium lines would be emitted from both regions. Liu (2003) showed that if H-deficient knots were present, one would expect to find that

$$T_e(\text{O II}) \lesssim T_e(\text{He I}) \lesssim T_e(\text{BJ}) \lesssim T_e([\text{O III}]), \quad (5)$$

where T_e(He I) is the temperature derived from the helium line ratios λ5876/λ4471 and λ6678/λ4471, which have a weak dependence on temperature, and T_e(O II) is the temperature derived from temperature-sensitive O II recombination line ratios. In this section we present measurements of T_e(He I) for the sample nebulae. The helium line emissivities were taken from Smits (1996), and the effects of collisional excitation from the metastable 2s ^{3}S level were corrected for using the formulae given by Kingdon & Ferland (1995). The temperatures we derive are given in Table 6. In almost every case they are lower than the temperatures derived from forbidden line diagnostics, and also lower than the hydrogen Balmer jump temperature. The temperatures derived from the λ5876/λ4471 ratio range from 1000 to 7960 K.

The value of T_e(He I) given by the λ5876/λ4471 line ratio is likely to be more reliable than the value derived from the λ6678/λ4471 line ratio, because the λ5876 line is roughly three times stronger, and the smaller wavelength difference means that the former ratio is less susceptible to flux calibration and reddening errors. Therefore, in subsequent analysis the temperature derived from λ5876/λ4471 is adopted as T_e(He I).

Table 6. Temperatures derived from helium line ratios λ5876/λ4471 and λ6678/λ4471.

Nebula	$T_{\lambda5876/\lambda4471}$	$T_{\lambda6678/\lambda4471}$
Cn 3–1	3400	4700
DdDm 1	3500	*
Hu 1–1	4740	9550
Hu 2–1	*	*
IC 2003	7670	1600
IC 351	4600	3790
IC 4846	*	13 400
IC 5217	3000	5100
M 1–73	7960	8820
M 1–74	3380	9200
M 3–34	*	17 000
Me 2–2	*	16 100
NGC 6803	4840	8100
NGC 6807	1000	*
NGC 6833	2440	14 100
NGC 6879	2340	3750
NGC 6891	3660	4100
NGC 7026	4120	4050
Sp 4–1	2440	3150
Vy 1–2	4430	3550
Vy 2–2	1890	7550

3.4 Temperatures derived from O II recombination lines

In general, the ratios of heavy element recombination lines depend very little on electron temperature. However, by comparing lines from different multiplets in which there is a difference in angular momentum, the temperature sensitivity is maximized. If the nebulae contain very cold ionized regions, the temperature measured from heavy element recombination lines should be close to the true temperature of the cold regions.

In this section we present measurements of the temperatures of the sample nebulae based on several O II line ratios. The ratios of the strongest 3s–3p and 3p–3d lines, λ4649 and λ4075 to the strong 3d–4f line λ4089 are likely to provide the most reliable temperatures as these three lines can only be produced by recombination from the 2p^2 ^{3}P$_2$ level of O^{2+}. The line ratios λ4414/λ4089 and λ4072/λ4089 are also used to derive temperatures, but in this case the lines form by recombination from different levels. Liu (2003) noted that for several nebulae, the latter line ratios implied temperatures considerably higher than the other O II diagnostics, and suggested that a possible explanation could be that the 2p^2 ^{3}P$_2$ level was underpopulated relative to its statistical equilibrium value, thus compromising the reliability of these line ratios as temperature diagnostics.

In Table 7 we give the temperature values derived from the line ratios λ4075/λ4089, λ4649/λ4089, λ4414/λ4089, λ4072/λ4089 and also for the ratio of the sum of the five strongest lines of the V1

Table 7. Temperatures derived from O II recombination line ratios.

Nebula	λ4075/λ4089	λ4649/λ4089	V1/λ4089	λ4072/λ4089	λ4414/λ4089	Adopted T_e(O II)
Cn 3–1	*	*	*	*	*	*
DdDm 1	*	*	*	*	*	*
Hu 1–1	*	*	*	*	*	*
Hu 2–1	1750	7460	7000	v low	>20 kK	4370
IC 1747	*	*	*	*	*	*
IC 2003	420	v low	120	v low	9110	270
IC 351	*	*	*	*	*	*
IC 4846	5830	v low	375	1400	*	2535
IC 5217	2500	v low	260	210	5220	990
M 1–73	v low	v low	*	v low	*	*
M 1–74	*	*	*	*	*	*
M 3–27	1100	6960	7910	v low	*	4030
M 3–34	900	4540	1000	>20kK	*	950
Me 2–2	2340	3390	3350	200	19 670	2850
NGC 6803	v low	2140	2500	3000	8270	2750
NGC 6807	2220	230	1100	100	19 150	1660
NGC 6833	1190	16 500	*	10 200	>20 kK	1190
NGC 6879	v low	v low	420	v low	*	420
NGC 6891	*	*	*	*	*	*
NGC 7026	1900	4580	6920	>20kK	18 430	4410
Sp 4–1	*	*	*	*	*	*
Vy 1–2	1250	3550	5250	8000	13 670	3250
Vy 2–2	v low	1510	1380	v low	>20 kK	1380

Table 8. Final adopted temperatures for the sample nebulae.

Nebulae	T_e([O III])	T_e(BJ)	T_e(He I)	T_e(O II)
Cn 3–1	7670	5090	3400	*
DdDm 1	12 300	8730	3500	*
Hu 1–1	12 110	8350	4740	*
Hu 2–1	9860	8960	*	4370
IC 1747	10 850	9650	*	*
IC 2003	12 650	8960	7670	270
IC 351	13 070	11 050	4600	*
IC 4846	10 710	7700	*	2535
IC 5217	11 270	11 350	3000	990
M 1–73	7450	5490	7960	*
M 1–74	10 150	7850	3380	*
M 3–27	13 000	9020	*	4030
M 3–34	12 230	8440	*	950
Me 2–2	10 970	10 590	*	2850
NGC 6803	9740	7320	4840	2750
NGC 6807	10 930	9900	1000	1660
NGC 6833	12 810	13 670	2440	1190
NGC 6879	10 400	8500	2340	420
NGC 6891	9330	5930	3660	*
NGC 7026	9310	7440	4120	4410
Sp 4–1	11 240	8830	2440	*
Vy 1–2	10 400	6630	4430	3250
Vy 2–2	13 910	9300	1890	1380

Table 9. Carbon CEL abundances.

Nebula	C^+/H^+ λ2326	C^{2+}/H^+ λ1908	C^{3+}/H^+ λ1550
Cn 3–1	*	*	*
DdDm 1	2.187e-6	5.949e-6	*
Hu 1–1	*	*	*
Hu 2–1	3.033e-4	3.135e-4	*
IC 1747	*	8.504e-4	*
IC 2003	*	1.685e-4	*
IC 351	*	9.629e-5	5.273e-5
IC 4846	1.484e-4	6.440e-5	*
IC 5217	2.493e-5	1.275e-4	4.822e-5
M 1–73	*	*	*
M 1–74	*	*	*
M 3–27	*	1.826e-4	*
M 3–34	*	*	*
Me 2–2	*	*	*
NGC 6803	*	1.573e-4	*
NGC 6807	*	*	*
NGC 6833	*	1.340e-5	*
NGC 6879	*	*	*
NGC 6891	*	1.983e-4	*
NGC 7026	*	2.021e-4	*
Sp 4–1	*	*	*
Vy 1–2	*	9.998e-5	1.121e-5
Vy 2–2	*	*	*

multiplet to the λ4089 line. The adopted O II temperature given is the average of those derived from the λ4075/λ4089 and V1/λ4089 ratios. The V1/λ4089 ratio is preferred to λ4649/λ4089, because the λ4649 line is blended with C III lines of comparable strength and thus its flux can be uncertain. In addition, Tsamis et al. (2003) and Ruiz et al. (2003) have shown that the relative intensities of O II V1 multiplet components are dependent on nebular density, in the sense that they deviate from local thermodynamic equilibrium (LTE) predictions for those nebulae having electron densities lower than the critical densities of the sublevels of the O^{2+} ^3P ground-state parent. Using all the lines from the V1 multiplet reduces the effects of any errors caused by line blending as well as the effects of deviations from LTE multiplet line ratios at low nebular densities.

It can be seen from Table 7 that, in many cases, very low temperatures are implied by O II line ratios, often $<10^3$ K. Such temperatures provide strong evidence for the existence of a very cold ionized component in planetary nebulae. The temperatures derived from the [O III] forbidden lines, the hydrogen Balmer jump, He I lines and O II recombination lines follow in almost every case the relation expected in the presence of cold, ionized, hydrogen-deficient material. The final adopted temperatures from these four diagnostics are given in Table 8.

4 ABUNDANCE ANALYSIS

In this section we present the abundances derived for the 23 sample nebulae, from both CELs and ORLs.

4.1 Ionic abundances from CELs

Abundances are derived for the sample nebulae from lines of C, N, O, Ne, S, Ar, Cl and Fe. To derive the abundances we adopt in all cases the [O III] temperature, in light of the uncertainties introduced into temperature determinations from singly ionized species by recombination excitation of the relevant lines.

The densities adopted were the average of the values implied by the diagnostics available, as listed in the final column of Table 4. IR lines often have critical densities comparable with typical nebular densities, and so any density variations present may significantly affect abundances derived from IR lines. For the nebulae analysed here, however, all the IR lines observed (listed in Appendix B) have critical densities much higher than the densities measured from the optical CEL diagnostics, and therefore the same electron density was adopted for both IR and optical abundance determinations from CELs.

The EQUIB code was used to solve the statistical equilibrium equations for multilevel atomic models, giving level populations and line emissivities for the appropriate physical conditions. The derived abundances are presented in Tables 9 (carbon), 10 (nitrogen), 11 (oxygen), 12 (neon), 13 (sulphur) and 14 (chlorine, argon and iron). The atomic data references used for the statistical calculations are listed in Appendix B.

4.2 Ionic abundances from ORLs

4.2.1 Helium abundances

Helium to hydrogen abundance ratios were derived using the hydrogen Balmer jump temperatures listed in Table 8 for all of the recombining ions, H^+, He^+ and He^{2+} (we note that the adoption instead for He^+ of the He I temperatures listed in Table 8 would lead to lower derived He^+ abundances). Effective recombination coefficients were taken from Brocklehurst (1972). Case A was assumed for the λ4471 and λ5876 triplets, and case B for the λ6678 singlet. Collisional effects were taken into account using the formulae derived by Kingdon & Ferland (1995). The results are presented in Table 15.

In most cases, the abundances derived from the three lines agree to within a few per cent. However, for two nebulae (DdDm 1 and

Table 10. Nitrogen CEL abundances.

Nebula	N^+/H^+ λ6548,6584	N^{2+}/H^+ λ1750
Cn 3–1	7.12e-5	*
DdDm 1	5.14e-6	*
Hu 1–1	2.73e-5	*
Hu 2–1	1.19e-5	*
IC 1747	7.58e-6	1.43e-4
IC 2003	2.44e-6	4.12e-5
IC 351	5.74e-7	*
IC 4846	3.45e-6	*
IC 5217	1.73e-6	4.76e-5
M 1–73	3.74e-5	*
M 1–74	7.82e-6	*
M 3–27	*	6.68e-5
M 3–34	4.65e-7	*
Me 2–2	2.40e-5	*
NGC 6803	1.82e-5	1.86e-4
NGC 6807	3.75e-6	*
NGC 6833	2.70e-6	*
NGC 6879	4.91e-7	*
NGC 6891	1.77e-6	*
NGC 7026	3.58e-5	*
Sp 4–1	2.96e-6	*
Vy 1–2	3.95e-6	9.30e-5
Vy 2–2	1.87e-6	*

Table 11. Oxygen CEL abundances.

Nebula	O^+/H^+ λ2470	O^+/H^+ λ3727,3729	O^+/H^+ λ7320,7330	O^{2+}/H^+ λ4959,5007
Cn 3–1	*	4.01e-4	5.39e-4	2.058e-5
DdDm 1	1.207e-5	2.80e-5	3.59e-5	8.417e-5
Hu 1–1	*	7.73e-5	*	2.506e-4
Hu 2–1	8.230e-5	6.97e-5	1.28e-4	2.542e-4
IC 1747	*	1.80e-5	5.70e-5	3.392e-4
IC 2003	*	7.37e-6	1.08e-5	1.809e-4
IC 351	*	1.87e-6	3.47e-6	1.870e-4
IC 4846	*	1.71e-5	2.86e-5	3.020e-4
IC 5217	*	9.49e-6	1.77e-5	2.900e-4
M 1–73	*	3.40e-4	2.99e-4	3.568e-4
M 1–74	*	3.26e-5	3.05e-5	3.636e-4
M 3–27	*	5.08e-7	*	3.990e-4[a]
M 3–34	*	2.52e-6	*	2.644e-4
Me 2–2	*	1.49e-5	3.28e-5	1.990e-4
NGC 6803	*	3.05e-5	5.06e-5	4.612e-4
NGC 6807	*	1.06e-5	2.11e-5	3.560e-4
NGC 6833	*	3.83e-6	3.46e-5	1.304e-4
NGC 6879	*	6.24e-6	*	3.198e-4
NGC 6891	*	1.25e-5	*	3.905e-4
NGC 7026	*	6.33e-5	6.41e-5	4.503e-4
Sp 4–1	*	1.50e-5	6.45e-5	1.420e-4
Vy 1–2	4.569e-5	1.36e-5	2.49e-5	4.155e-4
Vy 2–2	*	2.66e-6	1.32e-5	9.190e-5

[a]5007 flux not available; 4363 and 4959 lines used to derive abundance.

Table 12. Neon CEL abundances.

Nebula	Ne^{2+}/H^+ 15.5 μm	Ne^{2+}/H^+ λ3868,3967	Ne^{3+}/H^+ λ2423	Ne^{3+}/H^+ λ4724,4725
DdDm 1	*	1.305e-5	*	*
Hu 1–1	*	6.175e-5	*	6.390e-6
Hu 2–1	1.008e-5	2.221e-5	*	*
IC 1747	*	7.654e-5	*	*
IC 2003	*	3.624e-5	2.197e-5	4.193e-5
IC 351	*	3.643e-5	1.707e-5	2.599e-5
IC 4846	*	6.313e-5	*	*
IC 5217	*	6.083e-5	1.103e-5	1.238e-5
M 1–73	*	3.994e-5	*	*
M 1–74	*	8.229e-5	*	*
M 3–27	*	6.267e-5	*	*
M 3–34	*	4.572e-5	*	*
Me 2–2	4.881e-5	3.876e-5	*	*
NGC 6803	*	1.145e-4	*	*
NGC 6807	*	4.572e-5	*	*
NGC 6833	*	2.366e-5	*	*
NGC 6879	*	6.292e-5	*	*
NGC 6891	6.651e-5	6.935e-5	*	*
NGC 7026	*	1.272e-4	*	*
Sp 4–1	*	9.433e-6	*	*
Vy 1–2	*	8.218e-5	2.114e-5	1.112e-5
Vy 2–2	8.947e-6	1.670e-5	*	*

Table 13. Sulphur CEL abundances.

Nebula	S^+/H^+ λ4068,4076	S^+/H^+ λ6717,6731	S^{2+}/H^+ λ6312	S^{2+}/H^+ 18.7 μm
Cn 3–1	1.579e-7	2.139e-6	5.331e-6	*
DdDm 1	1.800e-7	1.713e-7	1.684e-6	*
Hu 1–1	8.519e-7	1.192e-6	3.020e-6	*
Hu 2–1	1.322e-7	4.541e-8	9.732e-7	1.589e-6
IC 1747	2.169e-7	1.940e-7	1.938e-6	*
IC 2003	1.378e-7	9.052e-8	1.132e-6	*
IC 351	*	2.231e-8	7.075e-7	*
IC 4846	1.668e-7	3.718e-7	1.922e-6	*
IC 5217	3.539e-7	9.985e-8	2.438e-6	*
M 1–73	4.417e-7	5.624e-7	*	*
M 1–74	4.894e-7	4.694e-7	4.580e-6	*
M 3–27	1.237e-7	*	*	*
M 3–34	6.140e-8	*	*	*
Me 2–2	1.982e-7	2.985e-8	8.553e-7	*
NGC 6803	8.187e-7	6.693e-7	5.176e-6	*
NGC 6807	1.767e-7	2.620e-7	2.935e-6	*
NGC 6833	4.391e-8	*	6.568e-7	*
NGC 6879	7.578e-8	*	2.951e-6	*
NGC 6891	*	*	*	5.170e-7
NGC 7026	1.018e-6	1.407e-6	7.841e-6	*
Sp 4–1	8.474e-8	5.024e-8	6.349e-7	*
Vy 1–2	1.429e-7	1.438e-7	2.467e-6	*
Vy 2–2	7.786e-8	3.753e-8	1.891e-6	*

NGC 6807) the abundance derived from the λ6678 line is much lower than that derived from the other lines. The problem cannot be accounted for by reddening errors – in both cases the intensity of the line is very low compared to λ4471 even before the correction for interstellar extinction. Another possible explanation is that there is a departure from pure case B recombination. Such a departure may be caused by the destruction of He I Lyman photons by dust grains or photoionization of neutral hydrogen. This mechanism is certainly plausible in the case of NGC 6807, for which high densities are implied by the standard diagnostics (34 000 cm^{-3} from the [Ar IV] λ4740/4711 ratio). Finally, underlying absorption may reduce the measured fluxes. Clegg, Peimbert & Torres-Peimbert (1987) find

Table 14. Chlorine and argon CEL abundances.

Nebula	Ar^{2+}/H^+ λ7135,7751	Ar^{2+}/H^+ 8.99 μm	Ar^{3+}/H^+ λ4711,4740	Ar^{4+}/H^+ λ7005	Cl^{2+}/H^+ λ5517,5537
Cn 3–1	6.580e-7	*	*	*	1.212e-7
DdDm 1	9.799e-8	*	9.756e-9	*	3.669e-8
Hu 1–1	*	*	1.093e-7	*	8.548e-8
Hu 2–1	4.650e-7	4.384e-7	7.901e-9	*	2.948e-8
IC 1747	8.219e-7	*	3.365e-7	*	*
IC 2003	3.902e-7	*	4.294e-7	*	3.687e-8
IC 351	3.021e-7	*	5.182e-7	6.464e-8	*
IC 4846	6.770e-7	*	1.824e-7	*	*
IC 5217	6.659e-7	*	5.165e-7	*	4.439e-8
M 1–73	2.050e-6	*	*	*	*
M 1–74	1.400e-6	*	1.830e-7	*	9.785e-8
M 3–27	*	*	1.230e-7	*	*
M 3–34	4.268e-7	*	5.169e-7	*	*
Me 2–2	4.968e-7	*	5.234e-8	*	4.165e-8
NGC 6803	1.699e-6	*	5.469e-7	*	1.454e-7
NGC 6807	1.063e-7	*	1.914e-7	*	4.378e-8
NGC 6833	5.922e-7	*	4.246e-8	*	*
NGC 6879	1.203e-6	*	4.588e-7	*	*
NGC 6891	1.253e-6	1.925e-6	1.063e-7	*	*
NGC 7026	1.612e-6	*	5.646e-7	*	1.381e-7
Sp 4–1	3.027e-7	*	1.024e-7	*	*
Vy 1–2	9.370e-7	*	6.902e-7	1.005e-7	*
Vy 2–2	6.792e-7	4.274e-7	6.640e-8	*	*

Table 15. Helium abundances.

Nebula	He^+/H^+ (4471)	(5876)	(6678)	Average	He^{2+}/H^+ (4686)	He/H
Cn 3–1	0.0442	0.0451	0.0432	0.045	*	0.045
DdDm 1	0.0877	0.0891	0.0373	0.089	*	0.089
Hu 1–1	0.0885	0.0900	0.0831	0.088	0.0142	0.103
Hu 2–1	0.0973	0.0781	0.0674	0.080	0.0002	0.080
IC 1747	0.1007	0.1033	0.1028	0.103	0.0109	0.114
IC 2003	0.0555	0.0522	0.0626	0.055	0.0427	0.098
IC 351	0.0607	0.0593	0.0613	0.060	0.0340	0.094
IC 4846	0.0966	0.0921	0.0845	0.091	0.0003	0.092
IC 5217	0.0876	0.0908	0.0846	0.089	0.0070	0.096
M 1–73	0.1154	0.1128	0.1112	0.113	0.0010	0.114
M 1–74	0.1010	0.1056	0.0938	0.102	0.0001	0.102
M 3–27	0.1239	*	*	0.123	*	0.123
M 3–34	0.0756	0.0651	0.0699	0.068	0.0187	0.087
Me 2–2	0.1365	0.1364	0.1471	0.139	0.0001	0.139
NGC 6803	0.1116	0.1111	0.1053	0.110	0.0034	0.114
NGC 6807	0.0816	0.0976	0.0202	0.094	0.0003	0.094
NGC 6833	0.0720	0.0742	0.0707	0.073	*	0.073
NGC 6879	0.0902	0.0967	0.0912	0.094	0.0022	0.097
NGC 6891	0.0900	0.0908	0.0898	0.090	*	0.090
NGC 7026	0.1015	0.1005	0.1014	0.101	0.0121	0.113
Sp 4–1	0.0891	0.0950	0.0925	0.093	0.0011	0.094
Vy 1–2	0.0850	0.0835	0.0867	0.084	0.0234	0.108
Vy 2–2	0.1015	0.1117	0.0941	0.106	0.0010	0.107

evidence for underlying absorption of He I lines in their study of DdDm 1.

The extremely low He/H abundance derived in the case of Cn 3–1 must be due to a considerable amount of neutral helium being present in this object. It is known to be an extremely low-excitation object (e.g. French 1981; Aller & Czyzak 1983), and this is evident in the current observations. The [O III] nebular lines are usually among the strongest in optical nebular spectra, with $I(\lambda4959+5007) \gg I(\mathrm{H}\beta)$, but in this case $I(\lambda4959+5007) \sim 0.25\, I(\mathrm{H}\beta)$. Zhang & Liu (2003) suggest using

$$\frac{\mathrm{He}}{\mathrm{H}} = \frac{\mathrm{S}^+ + \mathrm{S}^{2+}}{\mathrm{S}^{2+}} \frac{\mathrm{He}^+}{\mathrm{H}^+}, \tag{6}$$

to correct for the unobserved neutral helium; this yields a total He/H abundance of 0.063, which is still very low and is certainly still an underestimate. Alternatively, Peimbert & Costero (1969) suggest the following ionization correction factor (ICF):

$$\frac{\mathrm{He}}{\mathrm{H}} = \left[\left(0.87 \times \frac{\mathrm{S}}{\mathrm{S} - \mathrm{S}^+}\right) + \left(0.13 \times \frac{\mathrm{O}}{\mathrm{O} - \mathrm{O}^+}\right)\right] \left(\frac{\mathrm{He}^+}{\mathrm{H}^+}\right). \tag{7}$$

This formula yields the very high value of He/H = 0.173. An accurate determination of the total chemical abundances in Cn 3–1 would need detailed photoionization modelling, and the lack of knowledge of the helium ionization structure makes applying an empirical ICF very uncertain for this object. Therefore, only ionic abundances are given for Cn 3–1.

4.2.2 C^{2+}/H^+, C^{3+}/H^+ and C^{4+}/H^+

Recombination line C^2/H^+ abundances for the sample nebula were derived using the strong λ4267 line, recorded at high signal-to-noise in all spectra except that of the known carbon-poor (Clegg et al. 1987) halo planetary nebula DdDm 1. Abundances derived for this line have long been known to be high compared to those derived from the UV C III] λ1906,1908 lines, and this had led to its pure recombination origin being questioned (e.g. Barker 1982).

In high signal-to-noise spectra, it is possible to detect recombination lines from states higher than the 4f ^{2}F^o level, such as the 4f ^{2}F^o –ng ^{2}G series which feeds the λ4267 line. The relative intensities of these lines can be compared to the predictions of recombination theory to determine whether the λ4267 line can be safely attributed to recombination alone or whether some other process might be overpopulating the 4f ^{2}F^o level and leading to overestimated C^{2+}/H^+ abundances. Wesson et al. (2003) and Wesson & Liu (2004) have shown that for both Abell 30 and NGC 6543 the strengths of lines from high in the recombination ladder were in very good agreement with theoretical predictions. Unfortunately for the nebulae under consideration here, high-excitation lines are not seen in the majority of cases. A clear detection is found in only one case, M 1–73, where the λ6462 4f–6g line is seen. Relative to λ4267 = 1.000, the observed line strength is 0.112, which is in agreement within the errors with the predicted value of 0.103.

Although high excitation lines are not generally seen in our spectra, in the light of the very good agreement with theory found in this work for these lines in the cases of Abell 30 and NGC 6543, and for other nebulae such as M2–36 (Liu et al. 2001) and NGC 6153 (Liu et al. 2000), it seems very safe to attribute the λ4267 line flux to recombination alone. Given its good detection in all spectra and insensitivity to the assumption of case A or case B recombination, C^{2+}/H^+ abundances for the sample nebulae were derived from λ4267 only. The abundances determined are listed in Table 16.

C III lines are detected in all spectra except that of DdDm 1, where the blend of three C III and two O II lines in the 4650-Å region is detected but not well enough to be adequately fitted. This nebula is a known halo Type IV object, with much lower heavy element abundances than for typical galactic disc objects (e.g. Clegg et al. 1987; Torres-Peimbert et al. 1997). In the case of Sp 4–1, the λ4650 feature is swamped by a broad stellar emission line; the angular diameter

Table 16. C^{2+}/H^{+} recombination line abundances derived from C II λ4267.

Nebula	I(λ4267)	C^{2+}/H^{+} ($\times10^{-3}$)
Cn 3–1	0.123	0.128
DdDm 1	*	*
Hu 1–1	0.871	1.015
Hu 2–1	0.433	0.456
IC 1747	1.256	1.560
IC 2003	0.654	0.299
IC 351	0.637	0.666
IC 4846	0.150	0.140
IC 5217	0.236	0.167
M 1–73	0.598	0.593
M 1–74	0.435	0.494
M 3–27	0.210	0.165
M 3–34	0.281	0.196
Me 2–2	0.652	0.626
NGC 6803	0.643	0.612
NGC 6807	0.085	0.071
NGC 6833	0.063	0.047
NGC 6879	0.335	0.177
NGC 6891	0.529	0.545
NGC 7026	0.902	0.952
Sp 4–1	1.389	1.328
Vy 1–2	0.937	0.927
Vy 2–2	0.273	0.215

of the nebula was too small for a nebular spectrum excluding the central star to be extracted. However, the λ4187 line is detected and so a C^{3+}/H^{+} abundance can be derived for the nebula.

The agreement between abundances derived from the V1 multiplet and from the V18 λ4187 line is reasonable, and where both are available, the adopted C^{3+}/H^{+} abundance is the mean of the two values. The results are presented in Table 17.

Table 17. C^{3+}/H^{+} recombination line abundances for the sample nebulae.

Nebula	V1 λ4650		V18 λ4187		Adopted
	I_{obs}	$10^4 \times \frac{C^{3+}}{H^{+}}$	I_{obs}	$10^4 \times \frac{C^{3+}}{H^{+}}$	
Cn 3–1	0.212	0.838	0.028	0.492	0.665
DdDm 1	*	*	*	*	*
Hu 1–1	0.246	0.842	*	*	0.842
Hu 2–1	0.358	1.389	*	*	1.389
IC 1747	0.635	1.997	*	*	1.997
IC 2003	0.948	6.950	0.249	4.010	5.480
IC 351	0.443	1.736	0.240	4.218	2.977
IC 4846	0.186	0.818	*	*	0.818
IC 5217	0.195	1.045	0.057	0.953	0.999
M 1–73	0.752	3.123	*	*	3.123
M 1–74	0.087	0.308	*	*	0.308
M 3–27	0.432	2.164	*	*	2.164
M 3–34	0.393	2.124	*	*	2.124
Me 2–2	0.058	0.249	*	*	0.249
NGC 6803	0.143	0.614	0.086	1.506	1.060
NGC 6807	0.270	1.300	*	*	1.300
NGC 6833	0.036	0.186	*	*	0.186
NGC 6879	0.333	2.164	*	*	2.164
NGC 6891	0.047	0.187	*	*	0.187
NGC 7026	0.148	0.573	0.047	0.825	0.699
Sp 4–1	*	*	0.074	1.296	1.296
Vy 1–2	0.252	1.049	0.119	2.088	1.569
Vy 2–2	0.265	1.326	*	*	1.326

Table 18. C^{4+}/H^{+} recombination line abundances for the sample nebulae.

Nebula	I_{obs}(λ4658)	$10^5 \times \frac{C^{4+}}{H^{+}}$
IC 1747	0.302	7.432
IC 2003	0.435	6.042
IC 351	0.106	2.209
M 3–34	0.109	1.735
NGC 7026	0.099	2.083
Vy 1–2	0.177	3.510
Vy 2–2	0.622	10.54

The C IV line at 4658.64 Å is blended in many cases with [Fe III] at 4658.10 Å. Where no He^{2+} emission is seen, all the line flux is attributed to [Fe III]. If He^{2+} is seen and other [Fe III] lines are present, the contribution of [Fe III] to the line flux can be calculated using the abundance derived from the other [Fe III] lines. If no other [Fe III] lines are seen and He^{2+} is present, the line flux is attributed to C IV. Abundances derived from this line are presented in Table 18.

4.2.3 N^{3+}/H^{+} and N^{2+}/H^{+}

N III lines were detected from all nebulae in the sample, but effective recombination coefficients are available for only two lines, λ4379 and λ4640 (Péquignot et al. 1991). Abundances derived from the λ4640 line are invariably higher than those derived from λ4379, by factors ranging from 1.2 to 15. The former line can be strongly affected by continuum fluorescence (Ferland 1992), and so is not used in these abundance determinations. The λ4379 line is detected from 11 nebulae, and the abundances derived from it for these nebulae are shown in Table 19. N II lines were detected from 16 of the 23 sample nebulae, and abundances derived from them are given in Table 20.

4.2.4 O^{2+}/H^{+}

O II recombination lines are seen in all the nebulae in the sample, with several nebulae exhibiting particularly rich spectra with many lines visible. Abundances derived from them are presented in Table 21. As well as abundances derived from each individual line, the co-added intensities of lines within each multiplet seen are used to derive an abundance for the multiplet, and abundances for the 3d–4f transitions are derived from the co-added intensities of the 3d–4f lines visible in the spectra. The abundance derived from

Table 19. N^{3+}/H^{+} ($\times10^{-4}$) recombination line abundances.

Nebula	I_{obs} (λ4379)	N^{3+}/H^{+} ($\times10^{-4}$)
IC 2003	0.169	0.494
IC 351	0.152	0.666
IC 5217	0.112	0.371
M 3–34	0.300	0.988
Me 2–2	0.027	0.109
NGC 6803	0.255	1.021
NGC 6879	0.134	0.400
NGC 7026	0.382	1.691
Vy 1–2	0.546	2.263
Vy 2–2	0.053	0.186

Table 20. N^{2+}/H^{+} ($\times 10^{-3}$) recombination line abundances for the sample nebulae.

λ_o	Mult	I_{obs}	N^{2+}/H^{+}
Cn 3–1			
4607.16	V5	0.057	1.897
4621.39	V5	0.082	2.738
4630.54	V5	0.050	0.446
V5 3s ^{3}P^o – 3p ^{3}P		**0.296**	**1.098**
4803.29	V20	0.028	0.401
V20 3p ^{3}D – 3d ^{3}D^o			
Adopted			**0.750 ± 0.246**
DdDm 1			
4607.16	V5	0.140	4.695
Adopted			**4.695**
Hu 2–1			
4601.48	V5	0.017	0.450
4607.16	V5	0.032	1.061
4621.39	V5	0.027	0.898
4630.54	V5	0.071	0.631
V5 3s ^{3}P^o – 3p ^{3}P		**0.189**	**0.698**
Adopted			**0.698**
IC 2003			
4630.54	V5	0.040	0.331
Adopted			**0.331**
IC 5217			
4630.54	V5	0.022	0.198
Adopted			**0.198**
M 1–73			
4630.54	V5	0.251	2.261
4788.13	V20	0.072	1.809
Adopted			**2.035 ± 0.160**
M 3–27			
4630.54	V5	0.053	0.489
Adopted			**0.489**
M 3–34			
4678.14	V61b	0.077	0.645
Adopted			**0.645**
Me 2–2			
4621.39	V5	0.024	0.813
4630.54	V5	0.088	0.796
V5 3s ^{3}P^o–3p ^{3}P		**0.212**	**0.800**
3994.99	V12	0.031	0.606
V12 3s ^{1}P^o–3p ^{1}D		**0.031**	**0.606**
4041.31	V39b	0.042	0.201
4530.41	V58b	0.029	0.207
3d–4f		**0.071**	**0.203**
Adopted			**0.536 ± 0.144**
NGC 6803			
4630.54	V5	0.065	0.589
V5 3s ^{3}P^o – 3p ^{3}P		**0.156**	**0.589**
4803.29	V20	0.043	0.595
V20 3p ^{3}D – 3d ^{3}D^o		**0.104**	**0.595**
4237.05	V48b	0.043	0.483
4530.41	V58b	0.050	0.353
3d–4f		**0.093**	**0.403**
Adopted			**0.529 ± 0.051**
NGC 6807			
4607.16	V5	0.044	1.494
Adopted			**1.494**

Table 20 – *continued*

λ_o	Mult	I_{obs}	N^{2+}/H^{+}
NGC 6833			
4601.48	V5	0.009	0.243
Adopted			**0.243**
NGC 7026			
4601.48	V5	0.072	1.913
4607.16	V5	0.048	1.597
4630.54	V5	0.081	0.722
V5 3s ^{3}P^o – 3p ^{3}P		**0.301**	**1.117**
4041.31	V39b	0.082	0.432
4043.53	V39a	0.064	0.440
4176.16	V43a	0.072	0.807
4241..24,.78	V48b	0.069	0.551
4432.74	V55a	0.047	0.805
4530.41	V58b	0.037	0.291
4552.53	V58a	*	*
3d–4f		**0.371**	**0.505**
Adopted			**0.811 ± 0.216**
Sp 4–1			
4788.13	V20	0.129	3.196
Adopted			**3.196**
Vy 1–2			
4601.48	V5	0.058	1.559
4607.16	V5	0.024	0.807
V5 3s ^{3}P^o – 3p ^{3}P		**0.327**	**1.225**
4176.16	V43a	0.045	0.473
4241..24,.78	V48b	0.092	0.690
4432.74	V55a	0.099	1.594
4552.53	V58a	0.032	0.993
3d–4f		**0.268**	**0.973**
Adopted			**1.099 ± 0.089**
Vy 2–2			
4607.16	V5	0.087	2.945
4630.54	V5	0.074	0.672
V5 3s ^{3}P^o – 3p ^{3}P		**0.305**	**1.115**
Adopted			**1.115**

the V5 multiplet is invariably higher than the average derived from other multiplets; an unknown blend could be enhancing the strengths of the two lines at λ4415,4417, or there could be errors in the available recombination coefficients for this multiplet. In light of the probable unreliability of V5 abundances, the abundance adopted is the mean of the values for all 3–3 multiplets excluding V5, and the 3d–4f value.

4.2.5 Ne^{2+}/H^{+}

Neon ORLs are seen in the spectra of eight of the 23 sample nebulae. In most cases the only transitions seen are 3d–4f transitions, and recombination coefficients assuming intermediate coupling calculated by Storey (unpublished) are used to derive abundances from them. These coefficients assume that the three fine structure levels of the $2p^4\,{}^3P_{2,1,0}$ ground terms of Ne^{2+} are thermalized. However, the critical densities of the $^3P_1$ and $^3P_0$ levels are quite high ($>10^4$ cm^{-3}), and so at lower densities their level populations may depart from the thermal equilibrium values. The equilibrium level populations for the $^3P_{2,1,0}$ levels are in the ratio 1 : 0.6 : 0.2, but in the low-density limit the $^3P_{1,0}$ levels are completely unpopulated. The strongest 3d–4f transitions arise from the $^3P_2$ level, and so at low

Table 21. O^{2+}/H^{+} recombination line abundances for the sample nebulae.

λ_0	Mult	I_{obs}	O^{2+}/H^{+} ($\times 10^{-3}$)
			DdDm 1
4638.86	V1	0.043	0.436
4641.81	V1	0.048	0.193
4661.63	V1	0.051	0.404
V1 3s ^{4}P – 3p ^{4}D^o		**0.355**	**0.300**
4325.76	V2	0.069	4.691
4366.89	V2	0.077	0.979
V2 3s ^{4}P – 3p ^{4}P^o		**0.824**	**1.564**
4414.90	V5	0.068	1.717
V5 3s ^{2}P – 3p ^{2}D^o		**0.113**	**1.717**
4078.84	V10	0.041	1.113
V10 3p ^{4}D^o – 3d ^{4}F		**1.080**	**1.113**
Adopted			**0.992 ± 0.262**
			Hu 1–1
4638.86	V1	0.077	0.759
4641.81	V1	0.120	0.469
4649.13	V1	0.138	0.284
4650.84	V1	0.016	0.158
V1 3s ^{4}P – 3p ^{4}D^o		**0.451**	**0.371**
4414.90	V5	0.040	0.846
4416.97	V5	0.042	1.601
V5 3s ^{2}P – 3p ^{2}D^o		**0.088**	**1.116**
Adopted			**0.371**
			Hu 2–1
4638.86	V1	0.071	0.719
4641.81	V1	0.146	0.586
4649.13	V1	0.240	0.507
4650.84	V1	0.038	0.385
4661.63	V1	0.068	0.539
4673.73	V1	0.026	1.330
4676.24	V1	0.043	0.406
V1 3s ^{4}P – 3p ^{4}D^o		**0.638**	**0.539**
4317.14	V2	0.043	0.586
4319.63	V2	0.027	0.341
4349.43	V2	0.098	0.534
V2 3s ^{4}P – 3p ^{4}P^o		**0.263**	**0.500**
4414.90	V5	0.060	1.468
4416.97	V5	0.043	1.896
V5 3s ^{2}P – 3p ^{2}D^o		**0.109**	**1.609**
4069.62	V10	0.038	0.383
4069.89	V10	0.061	0.385
4072.16	V10	0.092	0.383
4075.86	V10	0.134	0.386
4085.11	V10	0.018	0.402
4092.93	V10	0.012	0.367
V10 3p ^{4}D^o – 3d ^{4}F		**0.370**	**0.385**
4129.32	V19	0.037	5.531
4132.80	V19	0.060	1.074
4153.30	V19	0.057	0.714
4169.22	V19	0.075	2.763
V19 3p ^{4}P^o – 3d ^{4}P		**0.287**	**1.351**
4110.78	V20	0.028	1.139
4119.22	V20	0.045	0.497
4120.28	V20	0.010	1.234
4120.54	V20	0.108	5.541
V20 3p ^{4}P^o – 3d ^{4}D		**0.300**	**1.339**
4705.35	V25	0.032	2.805
V25 3p ^{2}D^o – 3d ^{2}F		**0.053**	**2.805**
4906.83	V28	0.023	0.902
V28 3p ^{4}S^o – 3d ^{4}P		**0.073**	**0.902**

Table 21 – *continued*

λ_0	Mult	I_{obs}	O^{2+}/H^{+} ($\times 10^{-3}$)
			Hu 2–1
4089.29	V48a	0.058	0.443
4083.90	V48b	0.003	0.080
4087.15	V48c	0.012	0.338
4609.44	V92a	0.008	0.142
3d–4f		**0.081**	**0.312**
Adopted			**1.017 ± 0.274**
			IC 1747
4638.86	V1	0.094	0.907
4641.81	V1	0.155	0.593
4649.13	V1	0.222	0.447
4650.84	V1	0.105	1.014
V1 3s ^{4}P – 3p ^{4}D^o		**0.741**	**0.597**
4072.16	V10	0.186	0.780
V10 3p ^{4}D^o – 3d ^{4}F		**0.746**	**0.780**
4121.46	V19	0.037	1.330
V19 3p ^{4}P^o – 3d ^{4}P		**0.274**	**1.330**
4119.22,20.28,.54	V20	0.187	1.629
V20 3p ^{4}P^o – 3d ^{4}D		**0.355**	**1.629**
Adopted			**1.084 ± 0.207**
			IC 2003
4638.86	V1	0.059	0.725
4641.81	V1	0.092	0.448
4649.13	V1	0.152	0.389
4650.84	V1	0.054	0.663
4661.63	V1	0.102	0.981
V1 3s ^{4}P – 3p ^{4}D^o		**0.519**	**0.532**
4366.89	V2	0.151	2.093
V2 3s ^{4}P – 3p ^{4}P^o		**1.012**	**2.093**
4414.90	V5	0.046	2.443
V5 3s ^{2}P – 3p ^{2}D^o		**0.077**	**2.443**
4069.89	V10	0.500	3.125
4072.16	V10	0.143	0.590
4075.86	V10	0.206	0.588
4078.84	V10	0.060	1.626
4085.11	V10	0.028	0.619
V10 3p ^{4}D^o – 3d ^{4}F		**1.091**	**1.123**
4119.22	V20	0.205	2.166
4120.54	V20	0.044	2.158
V20 3p ^{4}P^o – 3d ^{4}D		**0.507**	**2.165**
4089.29	V48a	0.102	0.571
4083.90	V48b	0.071	1.389
4087.15	V48c	0.021	0.433
3d–4f		**0.194**	**0.697**
Adopted			**1.322 ± 0.343**
			IC 351
4638.86	V1	0.087	0.877
4641.81	V1	0.127	0.508
4649.13	V1	0.258	0.542
4650.84	V1	0.071	0.716
V1 3s ^{4}P – 3p ^{4}D^o		**0.698**	**0.588**
4132.80	V19	0.081	1.440
V19 3p ^{4}P^o – 3d ^{4}P		**0.308**	**1.440**
4609.44	V92a	0.067	1.178
Adopted			**1.069 ± 0.356**

densities their recombination coefficients may be underestimated by a factor of 1.8, with abundances derived from them correspondingly overestimated.

For the current sample, only 3d–4f abundances are available for most of the nebulae in which Ne II ORLs are detected. In one case, Vy 1–2, 3d–4f and 3s–3p transitions are detected, and the mean

Table 21 – *continued*

λ_0	Mult	I_{obs}	O^{2+}/H^+ ($\times10^{-3}$)
			IC 4846
4638.86	V1	0.052	0.527
4641.81	V1	0.139	0.559
4649.13	V1	0.189	0.400
4650.84	V1	0.067	0.680
4661.63	V1	0.072	0.571
4673.73	V1	0.022	1.126
4676.24	V1	0.062	0.586
V1 3s ^{4}P – 3p ^{4}D^o		**0.609**	**0.515**
4349.43	V2	0.203	1.100
V2 3s ^{4}P – 3p ^{4}P^o		**0.581**	**1.100**
4069.62	V10	0.079	0.781
4069.89	V10	0.127	0.787
4072.16	V10	0.191	0.782
4075.86	V10	0.276	0.782
4078.84	V10	0.140	3.765
4085.11	V10	0.051	1.118
4092.93	V10	0.036	1.081
V10 3p ^{4}D^o – 3d ^{4}F		**0.903**	**0.922**
4119.22	V20	0.354	3.798
4120.28	V20	0.032	3.834
4120.54	V20	0.076	3.785
V20 3p ^{4}P^o – 3d ^{4}D		**0.876**	**3.798**
4089.29	V48a	0.099	0.681
4087.15	V48c	0.082	2.080
3d–4f		**0.181**	**0.979**
Adopted			**1.463 ± 0.550**
			0.879 ± 0.11 if V20 excluded
			IC 5217
4638.86	V1	0.064	0.654
4641.81	V1	0.125	0.506
4649.13	V1	0.181	0.386
4650.84	V1	0.062	0.634
4661.63	V1	0.058	0.464
4673.73	V1	0.021	1.084
4676.24	V1	0.052	0.495
V1 3s ^{4}P – 3p ^{4}D^o		**0.592**	**0.504**
4349.43	V2	0.083	0.446
4366.89	V2	0.078	0.981
V2 3s ^{4}P – 3p ^{4}P^o		**0.323**	**0.606**
4414.90	V5	0.033	0.990
4416.97	V5	0.028	1.513
V5 3s ^{2}P – 3p ^{2}D^o		**0.065**	**1.176**
4069.62	V10	0.067	0.645
4069.89	V10	0.108	0.652
4072.16	V10	0.162	0.646
4075.86	V10	0.235	0.648
4085.11	V10	0.031	0.662
V10 3p ^{4}D^o – 3d ^{4}F		**0.652**	**0.649**
4153.30	V19	0.043	0.502
4156.53	V19	0.053	3.883
V19 3p ^{4}P^o – 3d ^{4}P		**0.220**	**0.966**
4089.29	V48a	0.097	0.576
4083.90	V48b	0.014	0.291
4087.15	V48c	0.028	0.614
4275.55,.99	V67	0.040	0.367
4277.43,.89	V67	0.035	0.897
4669.27,.43	V89b	0.012	1.770
3d–4f		**0.226**	**0.542**
Adopted			**0.653 ± 0.082**

Table 21 – *continued*

λ_0	Mult	I_{obs}	O^{2+}/H^+ ($\times10^{-3}$)
			M 1–73
4638.86	V1	0.217	2.195
4641.81	V1	0.343	1.375
4649.13	V1	0.329	0.694
4650.84	V1	0.087	0.880
4661.63	V1	0.106	0.839
V1 3s ^{4}P – 3p ^{4}D^o		**1.224**	**1.033**
4069.62	V10	0.100	0.994
4069.89	V10	0.160	0.998
4072.16	V10	0.240	0.988
4075.86	V10	0.347	0.989
4085.11	V10	0.045	0.992
4092.93	V10	0.032	0.966
V10 3p ^{4}D^o – 3d ^{4}F		**0.957**	**0.983**
4119.22,20.28,.54	V20	0.167	1.388
V20 3p ^{4}P^o – 3d ^{4}D		**0.317**	**1.388**
4906.83	V28	0.167	6.428
V28 3p ^{4}S^o – 3d ^{4}P		**0.529**	**6.428**[a]
4089.29	V48a	0.249	1.790
4083.90	V48b	0.028	0.704
4087.15	V48c	0.101	2.680
3d–4f		**0.378**	**1.746**
Adopted			**1.288 ± 0.150**
			M 1–74
4649.13	V1	0.309	0.641
4650.84	V1	0.058	0.580
4661.63	V1	0.084	0.654
4676.24	V1	0.063	0.583
V1 3s ^{4}P – 3p ^{4}D^o		**0.871**	**0.722**
4071.23,2.16	V48a,V10	0.190	0.731
Adopted			**0.727 ± 0.005**
			M 3–27
4638.86	V1	0.309	3.123
4641.81	V1	0.327	1.311
4649.13	V1	0.619	1.304
4650.84	V1	0.088	0.890
4661.63	V1	0.237	1.875
4673.73	V1	0.047	2.399
4676.24	V1	0.169	1.591
V1 3s ^{4}P – 3p ^{4}D^o		**1.796**	**1.530**
4069.62	V10	0.095	0.951
4069.89	V10	0.151	0.948
4072.16	V10	0.228	0.945
4075.86	V10	0.330	0.947
V10 3p ^{4}D^o – 3d ^{4}F		**0.916**	**0.947**
4319.63	V2	0.158	1.987
V2 3s ^{4}P – 3p ^{4}P^o		**1.048**	**1.987**
4089.29	V48a	0.069	0.517
4275.55,.99	V67a,b	0.325	3.761
4303.82,.61	V53a,V65a	0.286	4.562
3d–4f		**0.680**	**2.406**
Adopted			**1.718 ± 0.271**
			M 3–34
4638.86	V1	0.104	1.060
4641.81	V1	0.189	0.764
4649.13	V1	0.410	0.871
4650.84	V1	0.075	0.765
4661.63	V1	0.043	0.343
4673.73	V1	0.054	2.779
V1 3s ^{4}P – 3p ^{4}D^o		**0.972**	**0.826**
4349.43	V2	0.294	1.574
V2 3s ^{4}P – 3p ^{4}P^o		**0.842**	**1.574**

Table 21 – *continued*

λ_0	Mult	I_{obs}	O^{2+}/H^+ ($\times 10^{-3}$)
			M 3–34
4069.62	V10	0.164	1.572
4069.89	V10	0.262	1.575
4072.16	V10	0.396	1.571
4075.86	V10	0.243	0.667
4085.11	V10	0.170	3.612
V10 3p ^{4}D^o – 3d ^{4}F		**1.270**	**1.257**
4156.53	V19	0.163	11.87
V19 3p ^{4}P^o – 3d ^{4}P		**2.718**	**11.87**[b]
4089.29	V48a	0.113	0.665
4087.15	V48c	0.003	0.065
4303.82,.61	V53a,V65a	0.126	1.580
3d–4f		**0.242**	**0.819**
Adopted			**1.119 ± 0.160**
			Me 2–2
4638.86	V1	0.046	0.469
4641.81	V1	0.080	0.323
4649.13	V1	0.153	0.325
4650.84	V1	0.040	0.408
4661.63	V1	0.042	0.335
4673.73	V1	0.007	0.360
4676.24	V1	0.035	0.332
V1 3s ^{4}P – 3p ^{4}D^o		**0.407**	**0.346**
4319.63	V2	0.026	0.328
4325.76	V2	0.026	1.774
4349.43	V2	0.024	0.131
V2 3s ^{4}P – 3p ^{4}P^o		**0.153**	**0.291**
4414.90	V5	0.038	0.990
4416.97	V5	0.038	1.784
V5 3s ^{2}P – 3p ^{2}D^o		**0.081**	**1.273**
4069.62	V10	0.031	0.309
4069.89	V10	0.050	0.312
4072.16	V10	0.075	0.310
4075.86	V10	0.108	0.308
V10 3p ^{4}D^o – 3d ^{4}F		**0.301**	**0.310**
4129.32	V19	0.021	3.079
4132.80	V19	0.039	0.685
4153.30	V19	0.030	0.369
4156.53	V19	0.021	1.620
V19 3p ^{4}P^o – 3d ^{4}P		**0.152**	**0.702**
4110.78	V20	0.013	0.519
V20 3p ^{4}P^o – 3d ^{4}D		**0.118**	**0.519**
4089.29	V48a	0.045	0.317
4288.82	V53c	0.027	1.905
4275.55,.99,6.28	V67a,b	0.019	0.185
4276.75,7.43,.89	V67b,c	0.020	0.326
4317.14,.70	V2,V53a	0.026	0.312
4669.27,.42	V89b	0.002	0.350
3d–4f		**0.139**	**0.342**
Adopted			**0.418 ± 0.060**
			NGC 6803
4638.86	V1	0.156	1.580
4641.81	V1	0.309	1.241
4649.13	V1	0.511	1.079
4650.84	V1	0.140	1.418
4661.63	V1	0.144	1.142
4673.73	V1	0.015	0.767
4676.24	V1	0.104	0.982
V1 3s ^{4}P – 3p ^{4}D^o		**1.393**	**1.177**

Table 21 – *continued*

λ_0	Mult	I_{obs}	O^{2+}/H^+ ($\times 10^{-3}$)
			NGC 6803
4319.63	V2	0.033	0.414
4349.43	V2	0.191	1.035
4366.89	V2	0.111	1.408
V2 3s ^{4}P – 3p ^{4}P^o		**0.494**	**0.935**
4414.90	V5	0.070	1.821
4416.97	V5	0.070	3.280
V5 3s ^{2}P – 3p ^{2}D^o		**0.150**	**2.342**
4069.62	V10	0.058	0.574
4069.89	V10	0.526	3.265
4072.16	V10	0.351	1.439
4075.86	V10	0.281	0.797
4085.11	V10	0.079	1.925
4092.93	V10	0.058	1.743
V10 3p ^{4}D^o – 3d ^{4}F		**1.412**	**1.443**
4132.80	V19	0.079	1.377
4153.30	V19	0.090	1.098
4156.53	V19	0.064	4.900[c]
4169.22	V19	0.058	2.080
V19 3p ^{4}P^o – 3d ^{4}P		**0.296**	**1.357**
4119.22	V20	0.111	1.194
4120.28	V20	0.024	2.883
4120.54	V20	0.023	1.149
V20 3p ^{4}P^o – 3d ^{4}D		**0.300**	**1.303**
4089.29	V48a	0.164	1.143
4083.90	V48b	0.036	0.790
4087.15	V48c	0.053	1.362
4275.55,.99,6.28	V67a,b	0.084	0.904
4276.62,.75,.43	V67b,c,V53c	0.050	1.043
4317.14,.70	V2,V53a	0.055	0.655
4466.42	V86b	0.073	5.581
4669.27	V89b	0.001	0.313
4602.13	V92b	0.055	2.239
4609.44,10.20	V92a,c	0.091	1.122
3d–4f		**0.607**	**1.300**
Adopted			**1.253 ± 0.066**
			NGC 6807
4638.86	V1	0.040	0.407
4641.81	V1	0.140	0.564
4649.13	V1	0.149	0.316
4661.63	V1	0.053	0.422
4676.24	V1	0.043	0.407
V1 3s ^{4}P – 3p ^{4}D^o		**0.437**	**0.370**
4349.43	V2	0.075	0.405
V2 3s ^{4}P – 3p ^{4}P^o		**0.215**	**0.405**
4414.90	V5	0.049	1.357
4416.97	V5	0.055	2.745
V5 3s ^{2}P – 3p ^{2}D^o		**0.111**	**1.853**
4069.62	V10	0.041	0.402
4069.89	V10	0.066	0.405
4072.16	V10	0.099	0.401
4075.86	V10	0.143	0.401
V10 3p ^{4}D^o – 3d ^{4}F		**0.398**	**0.402**
4153.30	V19	0.053	0.633
V19 3p ^{4}P^o – 3d ^{4}P		**0.141**	**0.633**
4906.83	V28	0.054	2.019
V28 3p ^{4}S^o – 3d ^{4}P		**0.171**	**2.019**
4089.29	V48a	0.060	0.385
4609.44,10.20	V92a,c	0.042	0.477
3d–4f		**0.102**	**0.418**
Adopted			**0.708 ± 0.242**

Table 21 – *continued*

λ_0	Mult	I_{obs}	O^{2+}/H^+ ($\times10^{-3}$)
			NGC 6833
4638.86	V1	0.028	0.292
4641.81	V1	0.075	0.310
4649.13	V1	0.105	0.228
4650.84	V1	0.034	0.354
4661.63	V1	0.033	0.269
4673.73	V1	0.007	0.368
4676.24	V1	0.021	0.204
V1 3s ^{4}P – 3p ^{4}D^o		**0.306**	**0.266**
4317.14,.70	V2,V53a	0.013	0.155
4319.63	V2	0.019	0.242
V2 3s ^{4}P – 3p ^{4}P^o		**0.110**	**0.212**
4414.90	V5	0.024	0.712
4416.97	V5	0.018	0.963
V5 3s ^{2}P – 3p ^{2}D^o		**0.045**	**0.802**
4069.62	V10	0.021	0.208
4069.89	V10	0.034	0.211
4072.16	V10	0.051	0.209
4075.86	V10	0.042	0.119
V10 3p ^{4}D^o – 3d ^{4}F		**0.169**	**0.172**
4089.29	v48a	0.019	0.118
4669.27,.42	V89b	0.002	0.310
3d–4f		**0.021**	**0.126**
Adopted			**0.194 ± 0.026**
			NGC 6879
4641.81	V1	0.180	0.722
4649.13	V1	0.192	0.405
4650.84	V1	0.099	1.002
4661.63	V1	0.115	0.911
4673.73	V1	0.030	1.532
4676.24	V1	0.097	0.914
V1 3s ^{4}P – 3p ^{4}D^o		**0.786**	**0.664**
4069.62	V10	0.049	0.492
4069.89	V10	0.221	1.391
4072.16	V10	0.118	0.490
4075.86	V10	0.055	0.158
4092.93	V10	0.083	2.528
V10 3p ^{4}D^o – 3d ^{4}F		**0.577**	**0.598**
4119.22	V20	0.076	0.837
4120.28	V20	0.016	1.967
4120.54	V20	0.174	8.891^d
V20 3p ^{4}P^o – 3d ^{4}D		**0.209**	**0.930**
4089.29	V48a	0.125	0.946
3d–4f		**0.125**	**0.946**
Adopted			**0.785 ± 0.078**
			NGC 6891
4638.86	V1	0.080	0.807
4641.81	V1	0.148	0.592
4649.13	V1	0.208	0.438
4650.84	V1	0.113	1.140
4661.63	V1	0.114	0.900
4673.73	V1	0.040	2.038
4676.24	V1	0.070	0.659
V1 3s ^{4}P – 3p ^{4}D^o		**0.781**	**0.657**
4366.89	V2	0.048	0.609
V2 3s ^{4}P – 3p ^{4}P^o		**0.322**	**0.609**
4069.62,.89	V10	0.234	0.900
4072.16	V10	0.140	0.579
4075.86	V10	0.115	0.329
4078.84	V10	0.064	1.737
V10 3p ^{4}D^o – 3d ^{4}F		**0.604**	**0.622**

Table 21 – *continued*

λ_0	Mult	I_{obs}	O^{2+}/H^+ ($\times10^{-3}$)
			NGC 6891
4119.22	V20	0.045	0.492
V20 3p ^{4}P^o – 3d ^{4}D		**0.111**	**0.492**
Adopted			**0.595 ± 0.031**
			NGC 7026
4638.86	V1	0.157	1.586
4641.81	V1	0.356	1.426
4649.13	V1	0.498	1.049
4650.84	V1	0.164	1.657
4661.63	V1	0.150	1.186
4673.73	V1	0.008	0.408
4676.24	V1	0.092	0.866
V1 3s ^{4}P – 3p ^{4}D^o		**1.439**	**1.213**
4317.14	V2	0.089	1.209
4319.63	V2	0.062	0.780
4349.43	V2	0.132	0.717
4366.89	V2	0.096	1.220
V2 3s ^{4}P – 3p ^{4}P^o		**0.480**	**0.911**
4414.90	V5	0.107	2.637
4416.97	V5	0.056	2.486
V5 3s ^{2}P – 3p ^{2}D^o		**0.175**	**2.583**
4069.62	V10	0.192	1.923
4069.89	V10	0.308	1.933
4072.16	V10	0.465	1.927
4075.86	V10	0.320	0.918
V10 3p ^{4}D^o – 3d ^{4}F		**1.464**	**1.513**
4153.30	V19	0.093	1.157
4156.53	V19	0.082	6.406^e
V19 3p ^{4}P^o – 3d ^{4}P		**0.247**	**1.157**
4119.22	V20	0.252	2.766
4120.28	V20	0.022	2.696
4120.54	V20	0.055	2.802
V20 3p ^{4}P^o – 3d ^{4}D		**0.591**	**2.767**
4083.90	V48b	0.114	2.996
4089.29	V48a	0.137	1.029
4275-77	V53,65,67	0.227	1.437
4303.82,.61	V53a,V65a	0.077	1.232
4669.27,.42	V89b	0.009	1.679
4609.44	V92a	0.126	2.207
3d–4f		**0.690**	**1.515**
Adopted			**1.513 ± 0.244**
			Sp 4–1
4349.43	V2	0.056	0.302
4366.89	V2	0.073	0.922
V2 3s ^{4}P – 3p ^{4}P^o		**0.259**	**0.487**
4069.62	V10	0.058	0.572
4069.89	V10	0.093	0.575
4072.16	V10	0.140	0.571
4075.86	V10	0.056	0.158
V10 3p ^{4}D^o – 3d ^{4}F		**0.395**	**0.403**
4132.80	V19	0.021	0.365
V19 3p ^{4}P^o – 3d ^{4}P		**0.080**	**0.365**
4110.78	V20	0.087	3.433
4119.22	V20	0.259	2.776
4120.28,.54	V20	0.056	1.968
V20 3p ^{4}P^o – 3d ^{4}D		**0.631**	**2.733**
Adopted			**0.418 ± 0.029**

(excluding anomalously high V20 abundance)

abundance derived from the 3d–4f transitions is two times higher than the 3s–3p abundance. Vy 1–2 has a density of 2830 cm^{-3}, and so this discrepancy is probably caused by the effects of departure from thermal equilibrium noted above. For nebulae for which only

Table 21 – *continued*

λ_0	Mult	I_{obs}	O^{2+}/H^+ ($\times10^{-3}$)
			Vy 1–2
4638.86	V1	0.291	2.948
4641.81	V1	0.603	2.422
4649.13	V1	0.972	2.053
4650.84	V1	0.324	3.283
4661.63	V1	0.287	2.276
4673.73	V1	0.097	4.962
4676.24	V1	0.241	2.276
V1 3s ^{4}P – 3p ^{4}D^o		**2.843**	**2.403**
4349.43	V2	0.324	1.759
4366.89	V2	0.346	4.397
V2 3s ^{4}P – 3p ^{4}P^o		**1.344**	**2.549**
4414.90	V5	0.167	4.258
4416.97	V5	0.078	3.583
V5 3s ^{2}P – 3p ^{2}D^o		**0.262**	**4.017**
4069.62	V10	0.300	2.988
4069.89	V10	0.480	2.996
4072.16	V10	0.724	2.983
4075.86	V10	0.629	1.795
4085.11	V10	0.156	3.443
4092.93	V10	0.113	3.415
V10 3p ^{4}D^o – 3d ^{4}F		**2.530**	**2.600**
3882.19,.45	V12,V11	0.104	2.466
V11,V12		**0.270**	**2.466**
4121.46	V19	0.141	4.844
4132.80	V19	0.071	1.249
4153.30	V19	0.148	1.822
4156.53	V19	0.084	6.491
4169.22	V19	0.043	1.556
V19 3p ^{4}P^o – 3d ^{4}P		**0.506**	**2.344**
4119.22	V20	0.228	2.474
4120.28	V20	0.020	2.425
4120.54	V20	0.048	2.419
V20 3p ^{4}P^o – 3d ^{4}D		**0.561**	**2.463**
4089.29	V48a	0.283	2.035
4083.90	V48b	0.135	3.395
4087.15	V48c	0.133	3.529
4303.82,.61	V53a,V65a	0.221	3.383
4281.32	V53b	0.072	9.811
4294.78,.92	V53b	0.124	3.116
4291.25	V55	0.093	4.280
4275.55,.99	V67b	0.239	2.654
4277.43,.89	V67c	0.134	4.152
4285.69	V78b	0.071	2.689
4466.42,.59	V86b	0.084	5.008
4669.27,.42	V89b	0.044	7.853
4609.44	V92a	0.179	3.000
3d–4f		**1.812**	**3.130**
Adopted			**2.565 ± 0.092**
			Vy 2–2
4638.86	V1	0.080	0.829
4641.81	V1	0.181	0.744
4649.13	V1	0.289	0.624
4650.84	V1	0.046	0.477
4661.63	V1	0.083	0.674
4676.24	V1	0.056	0.541
V1 3s ^{4}P – 3p ^{4}D^o		**0.755**	**0.653**
4317.14	V2	0.080	1.099
4319.63	V2	0.081	1.030
4325.76	V2	0.095	6.529
4349.43	V2	0.089	0.489
V2 3s ^{4}P – 3p ^{4}P^o		**0.517**	**0.991**

Table 21 – *continued*

λ_0	Mult	I_{obs}	O^{2+}/H^+ ($\times10^{-3}$)
			Vy 2–2
4414.90	V5	0.152	4.397
4416.97	V5	0.135	7.035
V5 3s ^{2}P – 3p ^{2}D^o		**0.307**	**5.339**
4069.62	V10	0.054	0.536
4069.89	V10	0.086	0.534
4072.16	V10	0.130	0.534
4075.86	V10	0.094	0.267
V10 3p ^{4}D^o – 3d ^{4}F		**0.415**	**0.425**
4132.80	V19	0.058	1.000
4153.30	V19	0.095	1.146
V19 3p ^{4}P^o – 3d ^{4}P		**0.239**	**1.086**
4110.78	V20	0.044	1.729
4119.22	V20	0.059	0.628
4120.28	V20	0.006	0.713
4120.54	V20	0.016	0.791
V20 3p ^{4}P^o – 3d ^{4}D		**0.213**	**0.916**
4705.35	V25	0.029	2.447
V25 3p ^{2}D^o – 3d ^{2}F		**0.048**	**2.447**
4089.29	V48a	0.098	0.623
4087.15	V48c	0.036	0.844
4276.28,.62,75	V67b,V53c	0.127	2.623
4277.42,.89	V67b,c	0.053	1.451
4669.27	V89b	0.002	0.571
3d–4f		**0.316**	**1.085**
Adopted			**1.086 ± 0.227**

[a]V28 abundance excluded from average due to being based only on one weak line in a noisy region. [b]V19 abundance excluded from average as λ4156 line may be affected by blending. [c] λ4156 line excluded from multiplet abundance determination due to possible blending; with the line included the abundance is 1.614×10^{-3}. [d]Excluded from multiplet abundance due to blending with He I λ4120.86. [e]Line excluded from multiplet abundance determination due to possible blending.

3d–4f abundances are available, the Ne^{2+}/H^+ abundance should be considered an upper limit.

Ne^{2+}/H^+ abundances derived for the sample nebulae are given in Table 22.

5 TOTAL ELEMENTAL ABUNDANCES FROM CELS AND ORLS

From the ionic abundances derived in the previous section, total elemental abundances are derived, correcting for unseen ionization stages using the ionization correction factor scheme of Kingsburgh & Barlow (1994).

5.1 C/H

Total carbon abundances are derived in several ways. CEL abundances are derived for the nebulae for which UV spectra are available. If no C^{4+} is present, then C/H is given simply by the sum of C^+, C^{2+} and C^{3+} if all are seen. If C^+ is not seen, equation (8) is used; if only C^{2+} is seen, then equation (9) is used:

$$\frac{\mathrm{C}}{\mathrm{H}} = \frac{\mathrm{O}^+ + \mathrm{O}^{2+}}{\mathrm{O}^{2+}}\frac{\mathrm{C}^{2+} + \mathrm{C}^{3+}}{\mathrm{H}^+}, \quad (8)$$

$$\frac{\mathrm{C}}{\mathrm{H}} = \frac{\mathrm{O}}{\mathrm{O}^{2+}}\frac{\mathrm{C}^{2+}}{\mathrm{H}^+}. \quad (9)$$

Table 22. Ne^{2+}/H^+ recombination line abundances in the sample nebulae.

Nebula	λ_o	Mult	I_{obs}	Ne^{2+}/H^+
DdDm 1	4413.22	V65	0.068	2.944e-3
		3d–4f		**2.944e-3**
Hu 1–1	3694.21	V1	0.349	1.071e-3
		3s–3p		**1.071e-3**
IC 2003	4409.30	V55e	0.038	5.919e-4
		3d–4f		**5.919e-4**
M 3–34	4409.30	V55e	0.225	3.505e-3
		3d–4f		**3.505e-3**
NGC 6803	4391.99	V55e	0.048	4.969e-4
	4409.30	V55e	0.064	9.969e-4
	4413.22	V65	0.030	1.299e-3
		3d–4f		**9.309e-4**
NGC 6807	4409.30	V55e	0.027	4.206e-4
		3d–4f		**4.206e-4**
NGC 7026	4391.99	V55e	0.078	8.075e-4
	4397.99	V57b	0.040	1.198e-3
		3d–4f		**1.003e-3**
Vy 1–2	3694.21	V1	0.244	7.639e-4
		3s–3p		**7.639e-4**
	4219.74	V52a	0.076	1.418e-3
	4391.99	V55e	0.094	9.731e-4
	4409.30	V55e	0.105	1.636e-3
	4428.64	V60c	0.062	1.469e-3
	4430.94	V61a	0.059	2.161e-3
		3d–4f		**1.531e-3**

No C^+/H^+ abundance is available from ORLs. To derive total ORL abundances, the unseen C^+ is corrected for using $icf(C) = 1 + O^+/O^{2+}$, with C/H then given by

$$\frac{C}{H} = icf(C)\frac{(C^{2+} + C^{3+} + C^{4+})}{H^+}. \qquad (10)$$

In the case of DdDm 1, where only C^+ and C^{2+} abundances are available, no ionization correction is applied, in light of the relatively low degree of ionization implied by the oxygen ionic ratios and lack of He^{2+} in the nebula. For nebulae where He^{2+}/He is small, the λ4658 line, if detected, is attributed to [Fe III], as discussed in Section 4.2, and the total carbon abundance is derived from the above formula simply neglecting C^{4+}/H^+. Where UV spectra are available, an alternative means of correcting for the unseen C^+ is to assume that the C^+/C^{2+} ratio derived from CELs is also applicable to ORLs. However, Tsamis (2002) and Tsamis et al. (2004) find that, in general, carbon ionic ratios derived from CELs are not equal to those derived from ORLs. Therefore the ionization correction scheme is preferred.

Total carbon abundances from CELs are given in Table 23, and those from ORLs are given in Table 24.

Table 23. C/H abundances from CELs.

			CELs		
Nebula	C^+/H^+	C^{2+}/H^+	C^{3+}/H^+	ICF(C)	C/H
Cn 3–1	*	*	*	*	*
DdDm 1	2.187e-6	5.949e-6	*	1.000	8.136e-6
Hu 1–1	*	*	*	*	*
Hu 2–1	3.033e-4	3.135e-4	*	1.104	6.812e-4
IC 1747	*	8.504e-4	*	1.126	9.580e-4
IC 2003	*	1.685e-4	*	1.527	2.573e-4
IC 351	*	9.629e-5	5.273e-5	1.010	1.505e-4
IC 4846	1.484e-4	6.440e-5	7.103e-5	1.000	2.838e-4
IC 5217	2.493e-5	1.275e-4	4.822e-5	1.000	2.007e-4
M 1–73	*	*	*	*	*
M 1–74	*	*	*	*	*
M 3–27	*	1.826e-4	*	1.001	1.828e-4
M 3–34	*	*	*	*	*
Me 2–2	*	*	*	*	*
NGC 6803	*	1.573e-4	*	1.088	1.712e-4
NGC 6807	*	*	*	*	*
NGC 6833	*	1.340e-5	*	1.029	1.379e-5
NGC 6879	*	*	*	*	*
NGC 6891	*	1.983e-4	*	1.032	2.046e-4
NGC 7026	*	2.021e-4	*	1.230	2.486e-4
Sp 4–1	*	*	*	*	*
Vy 1–2	*	9.998e-5	1.121e-5	1.087	1.209e-4
Vy 2–2	*	*	*	*	*

Table 24. C/H abundances from ORLs.

			ORLs		
Nebula	C^{2+}/H^+	C^{3+}/H^+	C^{4+}/H^+	ICF(C)	C/H
Cn 3–1	1.276e-4	6.650e-5	*	20.49	3.977e-3
DdDm 1	*	*	*	*	*
Hu 1–1	1.015e-3	8.416e-5	*	1.308	1.438e-3
Hu 2–1	4.563e-4	1.389e-4	*	1.274	7.583e-4
IC 1747	1.560e-3	1.997e-4	7.432e-5	1.053	1.931e-3
IC 2003	2.992e-4	5.480e-4	6.042e-5	1.041	9.448e-4
IC 351	6.663e-4	2.977e-4	2.209e-5	1.010	9.960e-4
IC 4846	1.399e-4	8.183e-5	*	1.057	2.344e-4
IC 5217	1.670e-4	9.991e-5	*	1.033	2.757e-4
M 1–73	5.927e-4	3.123e-4	*	1.953	1.767e-3
M 1–74	4.938e-4	3.077e-4	*	1.090	8.736e-4
M 3–27	1.650e-4	2.164e-4	*	1.002	3.822e-4
M 3–34	1.962e-4	2.124e-4	1.735e-5	1.010	4.302e-4
Me 2–2	6.257e-4	2.487e-5	*	1.075	6.994e-4
NGC 6803	6.118e-4	1.060e-4	*	1.066	7.652e-4
NGC 6807	7.072e-5	1.300e-4	*	1.030	2.067e-4
NGC 6833	4.733e-5	1.858e-5	*	1.029	6.782e-5
NGC 6879	1.768e-4	2.164e-4	*	1.020	4.011e-4
NGC 6891	5.448e-4	1.875e-5	*	1.032	5.816e-4
NGC 7026	9.525e-4	6.988e-5	2.083e-5	1.141	1.190e-3
Sp 4–1	1.328e-3	1.296e-4	*	1.106	1.612e-3
Vy 1–2	9.268e-4	1.568e-4	3.510e-5	1.033	1.156e-3
Vy 2–2	2.150e-4	1.326e-4	1.054e-4	1.029	4.661e-4

5.2 N/H

Total nitrogen abundances are somewhat uncertain in the cases where only optical spectra are available. The only ionization stage which is then observed is N^+, which generally accounts for only a small fraction (⩽10 per cent) of the total nitrogen abundance. The unobserved ionization stages are corrected for by assuming that $N/N^+ = O/O^+$, so that $N/H = (O/O^+)(N^+/H^+)$.

Where UV spectra are available, the N/H abundance is more securely derived. The λ1750 N III] line is used to derive N^{2+}/H^+ abundances. The λ1486 N IV] line is not observed from any of the sample nebulae, and to account for the N^{3+} present in the nebula, the N^{3+}/N^{2+} ratio derived from ORLs is assumed to also apply to CELs.

Total ORL abundances are derived assuming that the N^+/N^{2+} ratio derived from CELs is applicable to ORLs. Where this ratio is

Table 25. N/H abundances from CELs and ORLs.

	CELs				ORLs			
Nebula	N^+/H^+	N^{2+}/H^+	ICF(N)	N/H	N^{2+}/H^+	N^{3+}/H^+	ICF(N)	N/H
Cn 3–1	7.12e-5	*	1.052	7.490e-5	7.500e-4	*	*	>7.500e-4
DdDm 1	5.14e-6	*	4.007	2.060e-5	4.695e-3	*	1.333	6.256e-3
Hu 1–1	2.73e-5	*	4.684	1.279e-4	*	*	*	*
Hu 2–1	1.19e-5	*	4.656	5.541e-5	6.980e-4	*	1.277	8.913e-4
IC 1747	7.58e-6	1.43e-4	21.23	1.609e-4	*	*	*	*
IC 2003	2.44e-6	4.12e-5	1.141	4.979e-5	3.310e-4	4.94e-5	1.052	4.000e-4
IC 351	5.74e-7	*	136.3	7.824e-5	*	6.66e-5	*	*
IC 4846	3.45e-6	*	18.71	6.455e-5	*	*	*	*
IC 5217	1.73e-6	4.76e-5	1.141	5.825e-5	1.980e-4	3.71e-5	1.031	2.423e-4
M 1–73	3.74e-5	*	2.062	7.712e-5	2.035e-3	*	1.965	3.999e-3
M 1–74	7.82e-6	*	12.16	9.509e-5	*	*	*	*
M 3–27	*	6.68e-5	1.002	6.690e-5	4.892e-4	*	1.002	4.899e-4
M 3–34	4.65e-7	*	124.5	5.789e-5	6.448e-4	9.88e-5	1.008	7.496e-4
Me 2–2	2.40e-5	*	14.36	3.446e-4	5.363e-4	1.09e-5	1.070	5.853e-4
NGC 6803	1.82e-5	1.86e-4	1.193	2.401e-4	5.287e-4	1.02e-4	1.082	6.824e-4
NGC 6807	3.75e-6	*	34.65	1.299e-4	1.494e-3	*	1.032	1.542e-3
NGC 6833	2.70e-6	*	35.04	9.461e-5	2.431e-4	*	1.029	2.501e-4
NGC 6879	4.91e-7	*	53.06	2.605e-5	*	4.00e-5	*	*
NGC 6891	1.77e-6	*	32.24	5.706e-5	*	*	*	*
NGC 7026	3.58e-5	*	8.749	3.132e-4	8.110e-4	1.69e-4	1.143	1.120e-3
Sp 4–1	2.96e-6	*	105.5	3.123e-4	3.196e-3	*	1.114	3.560e-3
Vy 1–2	3.95e-6	9.30e-5	1.206	1.161e-4	1.099e-3	2.26e-4	1.035	1.372e-3
Vy 2–2	1.87e-6	*	35.77	6.689e-5	1.115e-3	1.86e-5	1.028	1.165e-3

not available, we use the relation $N^+/N=O^+/O$ to correct for the N^+ present. Where only N^{2+}/H^+ abundances are available from ORLs, the ionization correction scheme of Kingsburgh & Barlow (1994) does not give a correction for the unseen ionization stages. In this case, N/H is estimating assuming $N/N^{2+} = O/O^{2+}$, based on the similarities of their ionization potentials. This relation is also used to derive the total N/H abundance from CELs for M 3–27, where only N^{2+}/H^+ is available, from UV observations.

Total N/H abundances from CELs and ORLs are presented in Table 25.

5.3 O/H

For CELs, given the possible strong effect of recombination on abundances derived from the λλ7320,7330 lines, O^+/H^+ abundances are derived from λλ3726,3729 only. Recombination can also be significant for these lines, and abundances derived from them may be considered upper limits. Given that O^+/O^{2+} is generally not large, the overall errors introduced into the O/H abundance by this possible uncertainty are small. The ionization correction factor for O is given by $[(He^+ + He^{2+})/He^+]^{2/3}$, following which O/H = ICF(O) $(O^+/H^+ + O^{2+}/H^+)$.

Only O^{2+}/H^+ abundances are available from ORLs, and to derive total oxygen abundances for ORLs, we assume that the value of O^+/O^{2+} derived from CELs is also applicable to ORLs. Total oxygen abundances are given in Table 26.

5.4 Ne/H

Total neon abundances are based on the derived values of Ne^{2+}/H^+ only. [Ne IV] lines are seen in the optical and/or UV in five cases, but the ionization correction scheme of Kingsburgh & Barlow (1994) does not provide an ICF equation for cases where Ne^{2+} and Ne^{3+} are the only ionization stages seen, and so instead total Ne/H abundances are derived using

$$\frac{\mathrm{Ne}}{\mathrm{H}} = \frac{\mathrm{O}}{\mathrm{O}^{2+}}\frac{\mathrm{Ne}^{2+}}{\mathrm{H}^+}. \tag{11}$$

The total Ne/H abundances thus derived are given in Table 27.

5.5 S/H, Cl/H and Ar/H

Sulphur, chlorine and argon abundances are available from CELs only. For sulphur, in most cases both S^+ and S^{2+} are seen. If both the λ6717,6731 and λ4068,4076 lines are seen, the S^+/H^+ abundance is taken from the λ6717,6731 lines only, as the λ4068,4076 lines are blended with O II lines of similar strength, and are probably also enhanced by recombination excitation. For M 3–27, M 3–34, NGC 6833 and 6879, S^+/H^+ is only available from λ4068,4076, and so the derived S/H may be overestimated.

Where both S^+ and S^{2+} are seen, S/H is derived using

$$\frac{\mathrm{S}}{\mathrm{H}} = \left[1-\left(1-\frac{\mathrm{O}^+}{\mathrm{O}}\right)^3\right]^{-1/3}\left(\frac{\mathrm{S}^+}{\mathrm{H}^+}+\frac{\mathrm{S}^{2+}}{\mathrm{H}^+}\right). \tag{12}$$

For M 1–73, M 3–27 and M 3–34, S^{2+} is not seen, and the following equation from Kingsburgh & Barlow (1994) is used to calculate its abundance from the observed S^+/H^+ abundance:

$$\frac{\mathrm{S}^{2+}}{\mathrm{S}^+} = 4.677 + \left(\frac{\mathrm{O}^{2+}}{\mathrm{O}^+}\right)^{0.433}. \tag{13}$$

Argon abundances are derived using the following equation in all except four cases:

$$\frac{\mathrm{Ar}}{\mathrm{H}} = \left[\frac{1}{1-(\mathrm{N}^+/\mathrm{N})}\right]\left(\frac{\mathrm{Ar}^{2+}}{\mathrm{H}^+}+\frac{\mathrm{Ar}^{3+}}{\mathrm{H}^+}+\frac{\mathrm{Ar}^{4+}}{\mathrm{H}^+}\right). \tag{14}$$

Table 26. O/H abundances from CELs and ORLs.

	CELs				ORLs		
Nebula	O^+/H^+	O^{2+}/H^+	ICF(O)	O/H	O^{2+}/H^+	ICF(O)	O/H
Cn 3–1	4.01e-4	2.058e-5	1.0005	4.218e-4	*	20.49	*
DdDm 1	2.80e-5	8.417e-5	1.0000	1.122e-4	1.174e-3	1.333	1.565e-3
Hu 1–1	7.73e-5	2.506e-4	1.1044	3.621e-4	0.743e-3	1.445	1.074e-3
Hu 2–1	6.97e-5	2.542e-4	1.0020	3.245e-4	1.082e-3	1.277	1.382e-3
IC 1747	1.80e-5	3.392e-4	1.0696	3.821e-4	1.084e-3	1.126	1.221e-3
IC 2003	7.37e-6	1.809e-4	1.4672	2.762e-4	1.509e-3	1.527	2.304e-3
IC 351	1.87e-6	1.870e-4	1.3494	2.549e-4	0.588e-3	1.363	8.014e-4
IC 4846	1.71e-5	3.020e-4	1.0024	3.199e-4	0.879e-3	1.059	9.309e-4
IC 5217	9.49e-6	2.900e-4	1.0519	3.150e-4	0.741e-3	1.086	8.047e-4
M 1–73	3.40e-4	3.568e-4	1.0060	7.010e-4	1.288e-3	1.965	2.531e-3
M 1–74	3.26e-5	3.636e-4	1.0007	3.965e-4	0.777e-3	1.090	8.469e-4
M 3–27	5.08e-7	3.990e-4	1.0000	3.995e-4	1.718e-3	1.002	1.721e-3
M 3–34	2.52e-6	2.644e-4	1.1755	3.138e-4	1.119e-3	1.187	1.328e-3
Me 2–2	1.49e-5	1.990e-4	1.0006	2.140e-4	0.540e-3	1.076	5.810e-4
NGC 6803	3.05e-5	4.612e-4	1.0208	5.019e-4	1.408e-3	1.088	1.532e-3
NGC 6807	1.06e-5	3.560e-4	1.0018	3.673e-4	0.871e-3	1.032	8.989e-4
NGC 6833	3.83e-6	1.304e-4	1.0000	1.342e-4	0.322e-3	1.029	3.313e-4
NGC 6879	6.24e-6	3.198e-4	1.0156	3.311e-4	0.785e-3	1.035	8.125e-4
NGC 6891	1.25e-5	3.905e-4	1.0000	4.030e-4	0.595e-3	1.032	6.140e-4
NGC 7026	6.33e-5	4.503e-4	1.0783	5.538e-4	1.666e-3	1.230	2.049e-3
Sp 4–1	1.50e-5	1.420e-4	1.0076	1.582e-4	0.418e-3	1.114	4.657e-4
Vy 1–2	1.36e-5	4.155e-4	1.1768	5.050e-4	2.747e-3	1.215	3.338e-3
Vy 2–2	2.66e-6	9.190e-5	1.0061	9.514e-5	1.718e-3	1.035	1.778e-3

Table 27. Total Ne/H abundances from CELs and ORLs.

	CELs			ORLs		
Nebula	Ne^{2+}/H^+	ICF(Ne)	Ne/H	Ne^{2+}/H^+	ICF(Ne)	Ne/H
DdDm 1	1.305e-5	1.333	1.740e-5	2.944e-3	1.333	3.924e-3
Hu 1–1	6.175e-5	1.445	8.923e-5	1.071e-3	1.445	1.548e-3
Hu 2–1	2.221e-5	1.277	2.836e-5	*	*	*
IC 1747	7.654e-5	1.126	8.618e-5	*	*	*
IC 2003	3.624e-5	1.527	5.534e-5	5.919e-4	1.527	9.038e-4
IC 351	3.643e-5	1.363	4.965e-5	*	*	*
IC 4846	6.313e-5	1.059	6.685e-5	*	*	*
IC 5217	6.083e-5	1.086	6.606e-5	*	*	*
M 1–73	3.994e-5	1.965	7.848e-5	*	*	*
M 1–74	8.229e-5	1.090	8.970e-5	*	*	*
M 3–27	6.267e-5	1.002	6.280e-5	*	*	*
M 3–34	4.572e-5	1.187	5.427e-5	*	*	*
Me 2–2	3.876e-5	1.076	4.171e-5	*	*	*
NGC 6803	1.145e-4	1.088	1.246e-4	9.309e-4	1.088	1.013e-3
NGC 6807	4.572e-5	1.032	4.718e-5	4.206e-4	1.032	4.155e-4
NGC 6833	2.366e-5	1.029	2.435e-5	*	*	*
NGC 6879	6.292e-5	1.035	6.512e-5	*	*	*
NGC 6891	6.935e-5	1.032	7.157e-5	*	*	*
NGC 7026	1.272e-4	1.230	1.565e-4	1.003e-3	1.230	1.234e-3
Sp 4–1	9.433e-6	1.114	1.051e-5	*	*	*
Vy 1–2	8.218e-5	1.215	9.985e-5	1.147e-3	1.215	1.394e-3
Vy 2–2	1.670e-5	1.035	1.728e-5	*	*	*

The exceptions are Hu 1–1 and M 3–27, for which only Ar^{3+} is seen and the following equation is used

$$\frac{\mathrm{Ar}}{\mathrm{H}} = \frac{\mathrm{Ne}}{\mathrm{Ne}^{2+}} \frac{\mathrm{Ar}^{3+}}{\mathrm{H}^+}, \tag{15}$$

and Cn 3–1 and M 1–73, in which only Ar^{2+} is seen, in which case the following equation applies:

$$\frac{\mathrm{Ar}}{\mathrm{H}} = 1.87 \left(\frac{\mathrm{Ar}^{2+}}{\mathrm{H}^+} \right). \tag{16}$$

Kingsburgh & Barlow (1994) do not give an ICF for chlorine. Liu et al. (2000) give the following equation based on the similarities between the ionization potentials of Cl and S ion stages:

$$\frac{\mathrm{Cl}}{\mathrm{H}} = \frac{\mathrm{S}}{\mathrm{S}^{2+}} \frac{\mathrm{Cl}^{2+}}{\mathrm{H}^{+}}. \tag{17}$$

Total Ar, S and Cl abundances derived from the above equations are given in Tables 28, 29 and 30, respectively.

Table 28. Total Ar/H abundances from CELs.

Nebula	Ar^{2+}/H^+	Ar^{3+}/H^+	Ar^{4+}/H^+	ICF(Ar)	Ar/H
Cn 3–1	6.580e-7	*	*	1.870	1.230e-6
DdDm 1	9.799e-8	9.756e-9	*	1.332	1.435e-7
Hu 1–1	*	1.093e-7	*	1.445	1.579e-7
Hu 2–1	4.650e-7	7.901e-9	*	1.274	6.025e-7
IC 1747	8.219e-7	3.365e-7	*	1.049	1.215e-6
IC 2003	3.902e-7	4.294e-7	*	1.087	8.909e-7
IC 351	3.021e-7	5.182e-7	6.464e-8	1.007	8.911e-7
IC 4846	6.770e-7	1.824e-7	*	1.056	9.075e-7
IC 5217	6.659e-7	5.165e-7	*	1.053	1.245e-6
M 1–73	2.050e-6	*	*	1.870	3.833e-6
M 1–74	1.400e-6	1.830e-7	*	1.090	1.725e-6
M 3–27	*	1.230e-7	*	1.001	1.230e-7
M 3–34	4.268e-7	5.169e-7	*	1.008	9.512e-7
Me 2–2	4.968e-7	5.234e-8	*	1.075	5.903e-7
NGC 6803	1.699e-6	5.469e-7	*	1.082	2.430e-6
NGC 6807	1.063e-7	1.914e-7	*	1.030	3.066e-7
NGC 6833	5.922e-7	4.246e-8	*	1.029	6.531e-7
NGC 6879	1.203e-6	4.588e-7	*	1.019	1.693e-6
NGC 6891	1.253e-6	1.063e-7	*	1.032	1.403e-6
NGC 7026	1.612e-6	5.646e-7	*	1.129	2.457e-6
Sp 4–1	3.027e-7	1.024e-7	*	1.105	4.476e-7
Vy 1–2	9.370e-7	6.902e-7	1.005e-7	1.035	1.788e-6
Vy 2–2	6.792e-7	6.640e-8	*	1.029	7.672e-7

Table 29. Total S/H abundances from CELs.

Nebula	S^{+}/H^+	S^{2+}/H^+	ICF(S)	S/H
Cn 3–1	2.139e-6	5.331e-6	*	*
DdDm 1	1.713e-7	1.684e-6	1.201	2.23e-6
Hu 1–1	1.192e-6	3.020e-6	1.249	5.26e-6
Hu 2–1	4.541e-8	9.732e-7	1.247	1.27e-6
IC 1747	1.940e-7	1.938e-6	1.950	4.16e-6
IC 2003	9.052e-8	1.132e-6	2.341	2.86e-6
IC 351	2.231e-8	7.075e-7	3.577	2.61e-6
IC 4846	3.718e-7	1.922e-6	1.874	4.30e-6
IC 5217	9.985e-8	2.438e-6	2.251	5.71e-6
M 1–73	5.624e-7	*	7.033	3.96e-6
M 1–74	4.694e-7	4.580e-6	1.639	8.28e-6
M 3–27	1.237e-7	*	21.74	2.69e-6
M 3–34	6.140e-8	*	45.75	2.81e-6
Me 2–2	2.985e-8	8.553e-7	1.725	1.53e-6
NGC 6803	6.693e-7	5.176e-6	1.800	1.05e-5
NGC 6807	2.620e-7	2.935e-6	2.282	7.30e-6
NGC 6833	4.391e-8	6.568e-7	2.291	1.61e-6
NGC 6879	7.578e-8	2.951e-6	2.622	7.94e-6
NGC 6891	*	*	2.230	*
NGC 7026	1.407e-6	7.841e-6	1.485	1.37e-5
Sp 4–1	5.024e-8	6.349e-7	1.570	1.08e-6
Vy 1–2	1.438e-7	2.467e-6	2.334	6.09e-6
Vy 2–2	3.753e-8	1.891e-6	2.306	4.45e-6

Table 30. Total Cl/H abundances from CELs.

Nebula	Cl^{2+}/H^+	ICF(Cl)	Cl/H
Cn 3–1	1.212e-7	*	*
DdDm 1	3.669e-8	1.324	4.86e-8
Hu 1–1	8.548e-8	1.742	1.49e-7
Hu 2–1	2.948e-8	1.305	3.85e-8
IC 1747	*	*	*
IC 2003	3.687e-8	2.527	9.32e-8
IC 351	*	*	*
IC 4846	*	*	*
IC 5217	4.439e-8	2.342	1.04e-7
M 1–73	*	*	*
M 1–74	9.785e-8	1.808	1.77e-7
M 3–27	*	*	*
M 3–34	*	*	*
Me 2–2	4.165e-8	1.789	7.45e-8
NGC 6803	1.454e-7	2.029	2.95e-7
NGC 6807	4.378e-8	2.487	1.09e-7
NGC 6833	*	*	*
NGC 6879	*	*	*
NGC 6891	*	*	*
NGC 7026	1.381e-7	1.747	2.41e-7
Sp 4–1	*	*	*
Vy 1–2	*	*	*
Vy 2–2	*	*	*

5.6 Total CEL and ORL abundances

Total abundances for the sample nebulae and averages for the sample are given in Table 31, together with the average CEL values derived for a southern sample by Kingsburgh & Barlow (1994), and solar abundances from Allende Prieto, Lambert & Asplund (2002), Allende Prieto & Lambert (2001) and Grevesse & Sauval (1998). Abundances are given on a logarithmic scale where N(H) = 12. The Type IV metal-deficient halo planetary nebula DdDm 1 is excluded from the average sample abundances. The average abundances derived for the current sample are slightly lower than those found by Kingsburgh & Barlow (1994). This is probably due to the radial metallicity gradient of the Milky Way: the sample of Kingsburgh & Barlow was of southern planetary nebulae and consisted mainly of nebulae inside the solar circle. The nebulae analysed here are all Northern hemisphere objects which are predominantly at larger galactocentric distances.

5.7 Comparison with previous results

Table 32 shows the results derived in this section alongside total elemental abundances determined previously. Only CEL abundances are compared; almost invariably only CEL abundances were derived in previous works, with the occasional exception of carbon abundances from the C II λ4267 line. Generally good agreement is seen between the results obtained in this work and previous determinations, with typical differences being 0.2 dex or less. Larger differences may be seen for S, Ar and Cl; discrepancies with previous studies for these elements are likely to arise because the lines used to derive these abundances are quite weak, and the ICFs used to derive total abundances are occasionally quite large, giving rise to further potential uncertainty.

Table 31. Total elemental abundances for all nebulae in the sample, on a logarithmic scale where N(H) = 12.

Nebula	He	C		N		O		Ne		S	Cl	Ar
	ORL	CEL	ORL	CEL	ORL	CEL	ORL	CEL	ORL	CEL	CEL	CEL
Cn 3–1	10.65	*	9.60	7.87	*	8.63	*	*	*	*	*	6.09
DdDm 1	10.95	6.91	*	7.31	9.79	8.05	9.19	7.24	9.59	6.35	4.69	5.16
Hu 1–1	11.01	*	9.16	8.11	*	8.56	9.03	7.95	9.19	6.72	5.17	5.20
Hu 2–1	10.90	8.83	8.88	7.74	8.95	8.51	9.14	7.45	*	6.10	4.59	5.78
IC 1747	11.06	8.98	9.29	8.21	*	8.58	9.09	7.94	*	6.62	*	6.08
IC 2003	10.99	8.41	8.98	7.70	8.60	8.44	9.36	7.74	8.96	6.46	4.97	5.95
IC 351	10.97	8.18	9.00	7.89	*	8.41	8.90	7.70	*	6.42	*	5.95
IC 4846	10.96	8.45	8.37	7.81	*	8.51	8.97	7.83	*	6.63	*	5.96
IC 5217	10.98	8.30	8.44	7.77	8.38	8.50	8.91	7.82	*	6.76	5.02	6.10
M 1–73	11.06	*	9.25	7.89	9.60	8.85	9.40	7.89	*	6.60	*	6.58
M 1–74	11.01	*	8.94	7.98	*	8.60	8.93	7.95	*	6.92	5.25	6.24
M 3–27	11.10	8.26	8.58	7.83	8.69	8.60	9.24	7.80	*	6.43	*	5.09
M 3–34	10.94	*	8.63	7.76	8.87	8.50	9.12	7.73	*	6.45	*	5.98
Me 2–2	11.14	*	8.84	8.54	8.77	8.33	8.76	7.62	*	6.18	4.87	5.77
NGC 6803	11.06	8.23	8.88	8.38	8.83	8.70	9.19	8.10	9.01	7.02	5.47	6.39
NGC 6807	10.97	*	8.32	8.11	9.19	8.57	8.95	7.67	8.62	6.86	5.04	5.49
NGC 6833	10.86	7.14	7.83	7.98	8.40	8.13	8.52	7.39	*	6.21	*	5.81
NGC 6879	10.99	*	8.60	7.42	*	8.52	8.91	7.81	*	6.90	*	6.23
NGC 6891	10.95	8.31	8.76	7.76	*	8.61	8.79	7.85	*	*	*	6.15
NGC 7026	11.05	8.40	9.08	8.50	9.05	8.74	9.31	8.19	9.09	7.14	5.38	6.39
Sp 4–1	10.97	*	9.21	7.49	9.55	8.20	8.67	7.02	*	6.03	*	5.65
Vy 1–2	11.03	8.08	9.06	8.06	9.14	8.70	9.52	8.00	9.14	6.78	*	6.25
Vy 2–2	11.03	*	8.67	7.83	9.07	7.98	9.25	7.24	*	6.65	*	5.88
Average	11.00	8.46	8.98	8.08	9.07	8.54	9.11	7.78	9.17	6.69	5.15	6.08
KB94[a]	11.06	8.74	*	8.35	*	8.68	*	8.09	*	6.92	*	6.39
Solar[b]	10.93	8.39	*	7.92	*	8.69	*	8.08	*	7.33	5.50	6.40

[a]Average values from Kingsburgh & Barlow (1994).
[b]Allende Prieto et al. (2002) (C/H), Allende Prieto & Lambert (2001) (O/H), Grevesse & Sauval (1998) (all others).

6 DISCUSSION

6.1 Abundance discrepancy factors

Abundance discrepancy factors for all ions where ORL and CEL abundances have been derived are shown in Table 33. In every case, the ionic abundances derived from ORLs are higher than those derived from CELs. It is evident that while the typical discrepancy factor is 2–3, some objects in this sample show much larger discrepancies. The ratio of the ORL to CEL O^{2+}/H^{+} abundance is the best determined adf, as it is derived from the optical spectra alone without the extra potential systematic errors involved in normalizing UV data to the same scale as the optical. IC 2003 and Vy 1–2 show moderately large discrepancies, with adf(O^{2+}) = 7.3 and 6.2, respectively, while DdDm 1 and Vy 2–2 show very large discrepancies, both with adf(O^{2+}) = 11.8.

The abundance discrepancies for ions of different elements are generally broadly similar, a pattern seen before for nebulae analysed by Liu et al. (1995, 2000, 2001) and Tsamis et al. (2004), and in the analysis of NGC 6543 by Wesson & Liu (2004). However, some systematic differences are seen. It is notable that adf(Ne^{2+}) is always larger than adf(O^{2+}), by factors of around 2. As discussed in Section 4.2.5, the assumption of thermal equilibrium for the $2p^4\,{}^3P_{2,1,0}$ fine structure levels of the ground term of Ne^{2+} may be unrealistic, resulting in overestimated abundance from 3d–4f transitions by factors of up to 1.8. As most of the Ne II lines observed in the sample nebulae are 3d–4f lines, it is likely that departures from thermal equilibrium are behind this discrepancy.

In the following sections, possible explanations for the observed ORL/CEL abundance discrepancies are considered.

6.2 Evidence for cold, H-deficient inclusions

The earliest interpretation of observed nebular temperature discrepancies was in terms of temperature fluctuations within the nebulae (Peimbert 1967, 1971). The mean temperature T_0 and the temperature fluctuation parameter t^2 were defined by Peimbert (1967) as

$$T_0(\mathrm{X}^{i+}) = \frac{\int T_\mathrm{e} N_\mathrm{e} N(\mathrm{X}^{i+})\,\mathrm{d}V}{\int N_\mathrm{e} N(\mathrm{X}^{i+})\,\mathrm{d}V}, \tag{18}$$

$$t^2(\mathrm{X}^{i+}) = \frac{\int (T_\mathrm{e} - T_0)^2 N_\mathrm{e} N(\mathrm{X}^{i+})\,\mathrm{d}V}{T_0^2 \int N_\mathrm{e} N(\mathrm{X}^{i+})\,\mathrm{d}V}. \tag{19}$$

Peimbert, Storey & Torres-Peimbert (1993) extended this interpretation to account for the ORL to CEL abundance discrepancies that they observed for three nebulae. However, as discussed previously, the temperature fluctuation scenario has serious difficulties, and cannot explain, for example, the good agreement between abundances derived from optical and IR CELs for NGC 6543 that was found by Wesson & Liu (2004). For the current sample, values of T_0 and t^2 can be derived from the difference between T_e([O III]) and T_e(BJ), under the assumption that the O^{2+} and H^{+} zones are co-extensive (for nebulae where the O^{+}/O^{2+} ratio is not small, mainly H II regions, the detailed treatment of Peimbert, Peimbert & Luridiana 2002 should instead be used). The effect this would have on abundance determinations can be calculated as follows. First, the

Table 32. Comparison of total elemental abundances derived here from CELs with those found in previous studies. References are as follows: AC83, Aller & Czyzak (1983); AK87, Aller & Keyes (1987); CAK96, Cuisinier, Acker & Köppen (1996); CPT87, Clegg et al. (1987); FHA96, Feibelman, Hyung & Aller (1996); H90, Henry (1990); HAFL01, Hyung et al. (2001a); HAL01, Hyung et al. (2001b); HKW96, Henry, Kwitter & Howard (1996); K70, Kaler (1970); K80, Kaler (1980); KH98, Kwitter & Henry (1998); KH01, Kwitter & Henry (2001); KPK87, Kaler, Pratap & Kwitter (1987); LAKC74, Lee et al. (1974); L81, Lutz (1981); TDPP97, Torres-Peimbert et al. (1997): WLB04, this paper.

Nebula	Ref	He	C	N	O	Ne	S	Ar	Cl
DdDm 1	WLB04	10.95	6.91	7.31	8.05	7.24	6.35	5.16	4.69
	KH98	11.00	6.73	7.55	8.07	7.15			
	TDPP97	*	7.15	7.40	8.18	7.32	6.53	5.86	*
	BC84	11.02	*	7.30	8.04	7.32	6.46	5.68	*
	CPT87	11.00	<7.23	7.39	8.15	7.30	6.53	5.86	*
Hu 1–1	WLB04	11.01	*	8.11	8.56	7.95	6.72	5.20	5.17
	K80	10.97	*	7.93	8.63	*	*	*	*
	AC83	11.02	*	8.15	8.73	7.96	7.13	6.26	5.10
Hu 2–1	WLB04	10.90	8.83	7.74	8.51	7.45	6.10	5.78	4.59
	K80	*	*	*	8.29	*	*	*	*
	L81	*	8.61	*	*	*	*	*	*
	HKW96	11.04	8.74	8.07	8.49	7.53	*	*	*
	AC83	10.95	*	7.60	8.48	7.48	6.13	5.90	4.51
IC 1747	WLB04	11.06	8.98	8.21	8.58	7.94	6.62	6.08	*
	K80	11.01	*	*	8.72	*	*	*	*
	AC83	11.05	*	8.30	8.75	8.05	6.90	6.33	5.34
IC 2003	WLB04	10.99	8.41	7.70	8.44	7.74	6.46	5.95	4.97
	K80	11.03	*	8.08	8.63	*	*	*	*
	AC83	10.98	*	8.04	8.62	7.89	6.59	6.29	5.10
IC 351	WLB04	10.97	8.18	7.89	8.41	7.70	6.42	5.95	*
	K80	10.99	*	7.93	8.59	*	*	*	*
	FHA96	10.99	8.45	7.84	8.61	7.63	6.69	6.00	4.75
	AC83	11.00	*	6.95	8.48	7.84	6.32	6.36	4.50
IC 4846	WLB04	10.96	8.45	7.81	8.51	7.83	6.63	5.96	*
	K80	10.94	*	7.98	8.64	*	*	*	*
	HAL01	10.98	7.74	7.88	8.60	7.90	6.95	6.18	5.11
	AC83	10.96	8.00	7.75	8.64	7.88	6.82	6.09	5.23
IC 5217	WLB04	10.98	8.30	7.77	8.50	7.82	6.76	6.10	5.02
	K80	10.98	*	8.01	8.53	*	*	*	*
	HAFL01	10.93	8.46	8.30	8.65	7.99	6.60	6.30	5.08
	AC83	11.00	*	8.02	8.70	7.93	7.23	6.35	5.30
	KH01	11.04	*	8.19	8.57	7.94	6.72	6.23	5.13
M 1–73	WLB04	11.06	*	7.89	8.85	7.89	6.60	6.58	*
	K70	11.37	*	*	8.26	*	*	*	*
M 1–74	WLB04	11.01	*	7.98	8.60	7.95	6.92	6.24	5.25
	K80	*	*	*	8.66	*	*	*	*
	AC83	11.02	*	8.11	8.71	8.11	7.15	6.54	5.35
	KH01	11.08	*	8.64	8.68	8.08	7.15	6.51	5.03
M 3–34	WLB04	10.94	*	7.76	8.50	7.73	6.45	5.98	*
	CAK96	10.95	*	6.91	8.54	*	6.38	5.86	4.59
Me 2–2	WLB04	11.14	*	8.54	8.33	7.62	6.18	5.77	4.87
	K80	11.21	*	8.56	8.26	*	*	*	*
	AK87	11.16	*	8.84	8.32	7.63	6.50	6.00	4.70
NGC 6803	WLB04	11.06	8.23	8.38	8.70	8.10	7.02	6.39	5.47
	K80	11.10	*	8.42	8.64	*	*	*	*
	LAKC74	11.09	*	8.64[a]	*	8.79	8.38[a]	6.43[a]	*
	AC83	11.10	*	8.49	8.77	8.37	7.11	6.91	*
NGC 6807	WLB04	10.97	*	8.11	8.57	7.67	6.86	5.49	5.04
	K80	11.01	*	*	8.36	*	*	*	*
	AK87	11.09	*	7.92	8.56	7.88	6.97	6.78	*

Table 32 – *continued*

Nebula	Ref	He	C	N	O	Ne	S	Ar	Cl
NGC 6833	WLB04	10.86	7.14	7.98	8.13	7.39	6.21	5.81	*
	AK87	11.00	*	8.13	8.05	7.34	6.20	5.70	*
	H90	10.90	*	8.04	8.03	7.28	*	*	*
NGC 6879	WLB04	10.99	*	7.42	8.52	7.81	6.90	6.23	*
	KPK87	10.96	*	7.69	8.61	7.84[a]	6.55[a]	5.84[a]	5.57[a]
	AK87	11.02	*	7.89	8.61	7.95	6.6	6.28	5.12
	KH01	11.04	*	7.96	8.58	7.92	6.53	6.17	4.74
NGC 6891	WLB04	10.95	8.31	7.76	8.61	7.85	*	6.15	*
	K80	11.08	*	7.59	8.44	*	*	*	*
	AK87	11.00	*	7.68	8.65	7.90	6.36	6.11	4.96
	KH01	11.04	*	7.75	8.63	7.92	6.26	6.21	4.83
NGC 7026	WLB04	11.05	8.40	8.50	8.74	8.19	7.14	6.39	5.38
	AC83	11.00	*	8.40	8.79	8.28	7.60	6.63	5.53
	KH01	11.15	*	8.74	8.86	8.35	7.19	6.72	5.56
Vy 1–2	WLB04	11.03	8.08	8.06	8.70	8.00	6.78	6.25	*
	K80	10.99	*	*	8.89	*	*	*	*
Vy 2–2	WLB04	11.03		7.83	7.98	7.24	6.65	5.88	*
	K80	11.16	*		7.85	*	*	*	*

[a]Total abundance derived from published ionic abundances and the KB94 ionization correction scheme.

Table 33. Abundance discrepancy factors for the sample nebulae.

Nebula	adf(O^{2+})	adf(N^{2+})	adf(C^{2+})	adf(C^{3+})	adf(Ne^{2+})
Cn 3–1	*	*	*	*	*
DdDm 1	11.8	*	*	*	*
Hu 1–1	2.97	*	*	*	*
Hu 2–1	4.00	*	1.46	*	*
IC 1747	3.20	*	1.83	1.09	*
IC 2003	7.31	8.10	1.78	5.12	16.6
IC 351	3.14	*	6.92	5.65	*
IC 4846	2.91	*	2.17	*	*
IC 5217	2.26	4.16	1.31	2.07	*
M 1–73	3.61	*	*	*	*
M 1–74	2.14	*	*	*	*
M 3–27	5.48	6.56	2.17	*	*
M 3–34	4.23	*	*	*	*
Me 2–2	2.10	*	*	*	*
NGC 6803	2.71	2.84	3.89	*	8.13
NGC 6807	2.00	*	*	*	8.91
NGC 6833	2.47	*	3.53	*	*
NGC 6879	2.46	*	*	*	*
NGC 6891	1.52	*	2.75	*	*
NGC 7026	3.36	*	4.71	*	7.94
Sp 4–1	2.94	*	*	*	*
Vy 1–2	6.17	11.8	9.27	14.0	13.8
Vy 2–2	11.8	*	*	*	*

values of T_0 and t^2 can be calculated from the observed values of T_e([O III]) and T_e(BJ) using the following equations:

$$T_e([\mathrm{O\,III}]_{na}) = T_0(\mathrm{O}^{2+}) \times \left\{1 + \frac{1}{2}\left[\frac{91380}{T_0(\mathrm{O}^{2+})} - 3\right] t^2(\mathrm{O}^{2+})\right\}, \quad (20)$$

$$T_e(\mathrm{BJ}) = T_0(\mathrm{H}^+)[1 - 1.67t^2(\mathrm{H}^+)]. \quad (21)$$

Then, the average line-emitting temperatures for [O III]λ4959,5007 and Hβ can be found using equations (8) and (9) of Peimbert et al. (2004)

$$T_{[\mathrm{O\,III}]} = T_0 \times \left\{1 + \left[\frac{(\Delta E/kT_0)^2 - (3\Delta E/kT_0) + 0.75}{(\Delta E/kT_0) - 0.5}\right]\frac{t^2}{2}\right\}, \quad (22)$$

$$T_{H\beta} = T_0\left[1 - (1-\alpha)\frac{t^2}{2}\right], \quad (23)$$

where $\Delta E = 28\,800$ K for [O III] λ4959,5007, and $\alpha = -0.633$ for Hβ. Finally, once the line-emitting temperatures are known, the factor by which accounting for temperature fluctuations would increase the derived O^{2+}/H^+ abundance can be found using equation (15) from Peimbert et al. (2004):

$$\frac{(\mathrm{O}^{2+}/\mathrm{H}^+)_{t^2\neq0}}{(O^{2+}/\mathrm{H}^+)_{t^2=0}} = \frac{T(\mathrm{H}\beta)^{-0.87}T([\mathrm{O\,III}])^{0.5}}{T_{5007/4363}^{-0.37}} \times \exp\left[\frac{\Delta E}{kT([\mathrm{O\,III}])} - \frac{\Delta E}{T_{5007/4363}}\right]. \quad (24)$$

Table 34 shows the values of T_0 and t^2 derived from the observed values of T_e(BJ) and T_e([O III]), the average line-emitting temperatures for [O III] and H I, and the increase $\Re$ in the value of O^{2+}/H^+ which would result from including the effect of t^2 in the abundance determinations. Column 7 gives the observed abundance discrepancy factor, and column 8 gives the ratio of adf/$\Re$. The nebulae IC 5217 and NGC 6833 are omitted from the table because they have measured Balmer jump temperatures slightly higher than their [O III] temperatures, and this analysis thus results in an unphysical negative value of t^2. For the other nebulae, it can be seen that, in almost every case, the increase in the O^{2+}/H^+ abundance resulting from the temperature fluctuations implied by T_e([O III]) and T_e(BJ) is smaller than the observed ORL/CEL discrepancy. This is especially true for the nebulae in the sample showing large values of adf(O^{2+}). For example, DdDm 1 has an adf(O^{2+}) of 12, but even though the Balmer jump temperature is almost 4000 K lower than the [O III] temperature, the implied temperature fluctuations would only increase the O^{2+}/H^+ CEL abundance by a factor of 1.9. Similarly, for Vy 2–2,

Table 34. The effect of temperature fluctuations on abundance determinations.

Nebula	T_0	t^2	$T_{H\beta}$	$T_{4959,5007}$	$\Re = \frac{(O^{2+}/H^+)_{t^2\neq0}}{(O^{2+}/H^+)_{t^2=0}}$	Observed adf(O^{2+})	$\frac{adf(O^{2+})}{\Re}$
Cn 3–1	5610	0.056	5350	6000	3.42	*	*
DdDm 1	10010	0.075	9390	10070	1.92	11.8	6.15
Hu 1–1	9640	0.080	9010	9750	2.06	2.97	1.44
Hu 2–1	9250	0.019	9100	9280	1.25	4.00	3.20
IC 1747	10080	0.025	9870	10090	1.28	3.20	2.50
IC 2003	10320	0.078	9660	10340	1.90	7.31	3.85
IC 351	11900	0.043	11480	11810	1.35	3.14	2.33
IC 4846	8630	0.064	8170	8810	2.05	2.91	1.42
M 1–73	5910	0.042	5700	6190	2.52	3.61	1.43
M 1–74	8550	0.049	8200	8690	1.79	2.14	1.20
M 3–27	10520	0.084	9800	10530	1.94	5.48	2.82
M 3–34	9760	0.080	9120	9850	2.04	4.23	2.07
Me 2–2	10730	0.008	10650	10720	1.08	2.10	1.94
NGC 6803	8020	0.051	7680	8210	1.96	2.71	1.38
NGC 6807	10270	0.021	10090	10270	1.23	2.00	1.63
NGC 6879	9120	0.040	8820	9200	1.55	2.46	1.59
NGC 6891	6760	0.072	6360	7150	3.12	1.52	0.49
NGC 7026	7980	0.040	7710	8130	1.72	3.36	1.95
Sp 4–1	9660	0.051	9250	9720	1.64	2.94	1.79
Vy 1–2	7670	0.080	7160	8000	2.77	6.17	2.23
Vy 2–2	11120	0.097	10230	11030	1.99	11.8	5.93

which also has adf(O^{2+}) = 12, the temperature fluctuations implied by T_e([O III]) $-T_e$(BJ) would only increase the O^{2+}/H^+ CEL abundance by a factor of 2.0. This demonstrates that simple temperature fluctuations cannot be the only cause of the observed abundance discrepancy.

Further evidence that temperature fluctuations alone cannot resolve the observed abundance discrepancies exists for the nebulae for which IR observations exist. As mentioned earlier, the very low excitation energies of IR fine structure lines ($E_x \leqslant 1000$ K) means that abundances derived from them are insensitive to temperature variations at typical nebular temperatures of 8000–15 000 K. Therefore, in the presence of temperature fluctuations they should give higher ionic abundances than optical and UV CELs. Instead, for the four nebulae for which *ISO* observations were available, very good agreement is seen between abundances derived from optical and IR CELs. For example, Hu 2–1 shows a moderately large adf(O^{2+}) of 6.97, but the Ar^{2+}/H^+ abundance derived from optical CELs is almost identical to the IR CEL abundance, while the Ne^{2+}/H^+ and O^{2+}/H^+ abundances derived from IR CELs are somewhat lower than those derived from optical CELs, the opposite of what would be expected in the temperature fluctuation scenario. Similarly, for Me 2–2, the Ne^{2+}/H^+ abundances derived from IR and optical CELs differ by only 25 per cent, while the observed adf(O^{2+}) is almost a factor of 3.

The case of NGC 6891 is interesting, as here the temperature fluctuations implied by the observed difference between T_e([O III]) and T_e(BJ) could account for the derived abundance discrepancies. However, looking at the IR CELs, no clear picture emerges. The Ar^{2+}/H^+ abundance derived from the [Ar III] 8.99-μm line is 50 per cent higher than that derived from the optical [Ar III] lines, in line with the observed adf(O^{2+}) of 1.52. However, the [Ne III] 15.5-μm IR line and λ3868,3967 optical CELs give Ne^{2+}/H^+ abundances which are in excellent agreement.

Finally, the nebula Vy 2–2 has a large adf(O^{2+}) of 11.8, but in this case the [Ne III] and [Ar III] IR CELs give abundances for Ne^{2+}/H^+ and Ar^{2+}/H^+ which are somewhat lower than the corresponding values derived from optical CELs. This is the opposite of what would be expected if temperature fluctuations were the cause of the observed discrepancy.

The analysis of the current sample points instead towards chemical inhomogeneities within the nebulae. The strongest evidence in favour of this hypothesis is the observed relation between the various temperatures derived from CELs, the hydrogen Balmer jump, He I emission-line ratios and O II recombination line ratios, as discussed in Section 3.2. If the observed abundance and temperature discrepancies were caused by temperature variations in a chemically homogeneous nebula, one would expect that the CEL temperature diagnostics would give a temperature weighted towards the hottest regions, while the recombination process temperature diagnostics would all be weighted towards the cooler regions in a similar way. There would be no reason to expect that T_e(O II) would be less than T_e(He I), which would in turn be less than T_e(BJ). This temperature relation is observed in every case in the current sample, and the only obvious way such a temperature relation can be produced is if the lower temperature regions are also enriched in heavy elements and helium.

If knots enriched in heavy elements are present within planetary nebulae, the high CNO abundances within them would result in strong cooling and a low temperature within them. In this case, T_e([O III]) would be most representative of the hot normal component of the nebula, while the temperature given by oxygen recombination lines would be a more direct measure of the temperature in the coldest regions of the nebula. The relative amounts of hydrogen and helium in the warm and cold components of the nebula would determine the temperatures measured from the Balmer jump and He I lines, which would then not necessarily be representative of any real part of the nebula.

Wesson et al. (2003) showed that the H-deficient knots of Abell 30 contain some extremely H-deficient material at very low temperatures. Possible links between A30 and other nebulae in which H-deficient knots are not directly observed are discussed further below.

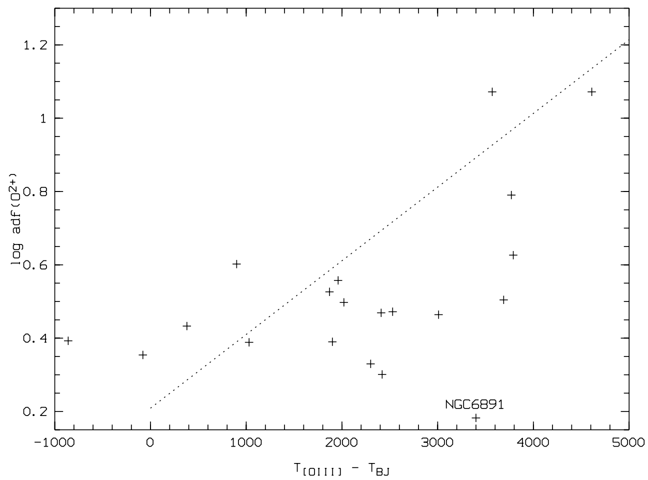

Figure 8. The ORL/CEL discrepancy for O^{2+} versus T_e([O III]) $-T_e$(BJ).

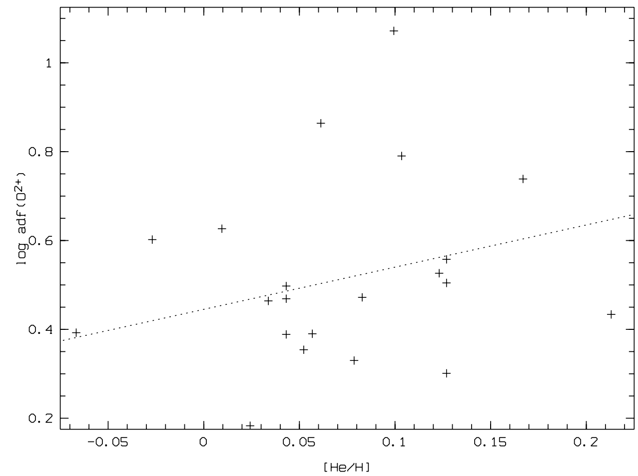

Figure 9. ORL/CEL discrepancy for O^{2+} versus He/H.

6.3 Correlations with nebular properties

6.3.1 Relation between adf(O^{2+}) and the temperature discrepancy

Liu et al. (2001) and Tsamis et al. (2004) have both found that the abundance discrepancy factor for O^{2+} [adf(O^{2+})] is tightly correlated with the difference between T_e([O III]) and T_e(BJ). The current results follow a similar trend, although with somewhat larger scatter than previously found. The extra scatter is most likely predominantly due to the errors inherent in the measurement of the Balmer jump temperature. Fig. 8 shows adf(O^{2+}) against T_e([O III]) $-T_e$(BJ) for the current sample, with the dashed line showing the fit found by Liu et al. (2001) to their data. NGC 6891 appears to lie well below the expected line, having a large difference between T_e([O III]) and T_e(BJ) but only a small adf(O^{2+}) of 1.52. The Balmer jump temperature seems well determined in this object, with good signal-to-noise in the continuum at around 3500 Å, and so the temperature discrepancy does not seem to have been overestimated. The abundance determinations also seem very reliable, with the ORL O^{2+}/H^{+} abundance based on four detected multiplets which give abundances in excellent agreement with each other.

6.3.2 A relation between adf(O^{2+}) and He/H?

Fig. 9 shows adf(O^{2+}) plotted against the total helium abundance He/H. Although the scatter is large, some evidence for a positive correlation of the adf with helium abundance is seen. The dashed line in the figure represents a linear fit to the data, with log adf(O^{2+}) $= 0.446 + 0.961$[He/H]. The correlation coefficient $r = 0.25$. A correlation was suggested by Zhang et al. (2004), and could arise because of uncertainties introduced into helium abundance determinations by the presence of H-deficient knots. As helium abundances are derived from recombination lines, the derived helium abundance will be overestimated if H-deficient knots are present as an appreciable amount of helium line emission will arise in the cooler component. Bi-abundance photoionization models by Péquignot et al. (2003) showed that the helium abundance can be overestimated in the presence of a cold H-deficient component. Given that the only helium lines seen in optical spectra are those formed by recombination, the fraction of helium emission from the hot and cold components is unknown. Observations of the near-infrared He I λ10830 line, which is partially collisionally excited, could lead to a more accurate determination of the true helium abundance, which is otherwise rendered uncertain by the presence of H-deficient knots.

6.4 C/O and N/O ratios

Table 35 shows the C/O and N/O elemental ratios derived from ORLs and from CELs for the sample nebulae. In most cases the ORL and CEL ratios are quite similar, but in some cases large discrepancies exist. For N/O, a few objects show a much larger N/O ratio from ORLs than from CELs. This discrepancy is present in the N^{2+}/O^{2+} ratios, the dominant ions of N and O. If the enhanced ORL abundances seen in the sample are due to H-deficient regions within the nebula, the higher ORL N/O ratios might point to a different chemical composition for these regions, and may suggest that they are highly processed material ejected by the central star.

Kingsburgh & Barlow (1994) define a Type I planetary nebula as one in which dredged-up carbon has been converted by envelope

Table 35. C/O and N/O ratios from ORLs and CELs in the sample nebulae.

Nebula	C/O (CELs)	C/O (ORLs)	N/O (CELs)	N/O (ORLs)
Cn 3–1	*	*	*	*
DdDm 1	0.07	*	0.18	4.00
Hu 1–1	*	1.34	0.35	*
Hu 2–1	0.48	0.55	0.17	0.65
IC 1747	*	1.58	0.42	*
IC 2003	0.93	0.41	0.18	0.17
IC 351	0.59	1.24	0.31	*
IC 4846	0.89	0.25	0.20	*
IC 5217	0.64	0.34	0.19	0.30
M 1–73	*	0.70	0.11	1.58
M 1–74	*	1.03	0.24	*
M 3–27	0.27	0.22	0.21	2.85
M 3–34	*	0.32	0.18	0.56
Me 2–2	*	1.20	1.61	1.01
NGC 6803	0.34	0.50	0.48	0.45
NGC 6807	*	0.23	0.35	1.72
NGC 6833	0.10	0.21	0.71	0.76
NGC 6879	*	0.49	0.08	*
NGC 6891	0.51	0.95	0.14	*
NGC 7026	*	0.58	0.57	0.55
Sp 4–1	*	3.46	0.20	0.76
Vy 1–2	0.24	0.35	0.23	0.41
Vy 2–2	*	0.26	0.70	0.66

burning into nitrogen, resulting in an N/O ratio greater than the (C+N)/O of H II regions within the host galaxy of the planetary nebula. For our Galaxy, (C+N)/O = 0.8, and so Me 2–2 qualifies as a Type I planetary nebula according to both CEL and ORL N/O ratios. DdDm 1, M 1–73, M 3–27 and NGC 6807 have ORL ratios which imply that they are Type I, but have non-Type I CEL ratios.

6.5 Possible origins of inclusions

Wesson et al. (2003) showed that the centre of the knots in Abell 30 must consist of extremely hydrogen-deficient material at very low temperatures, and subsequent three-dimensional photoionization modelling of the knots (Ercolano et al. 2003) showed that this was a physically plausible situation, with the very high CNO abundances in the core of the knot strongly cooling the material and giving rise to the very low temperatures of the ionized gas. There is very good evidence from the sample of nebulae analysed in this paper that hydrogen-deficient material exists in many if not all planetary nebulae. Such material may have a similar origin to the knots of Abell 30.

Wesson et al. (2003) discussed some of the problems with the born-again theory of Iben, Kaler & Truran (1983). Most importantly, the born-again theory predicts carbon-rich knots, whereas both CELs and ORLs give C/O <1 for the knots in Abell 30. In the current sample, 17 out of 23 nebulae also have a C/O ratio less than unity, with only one (Sp 4–1) having a ratio substantially greater than 1, indicating that an ejection of material in a very late helium flash is unlikely to be the origin of H-deficient regions in most planetary nebulae.

The collinearity of the two polar knots with the central star in A30 is also very hard to explain in a single star scenario, and suggests instead an accretion disc within a double star system. Recently, De Marco et al. (2004) have suggested that a large fraction of planetary nebula central stars may be spectroscopic binaries. They found radial velocity variations in 10 out of 11 planetary nebula central stars analysed, although without confirming that the variation was periodic. If a majority of planetary nebulae contain a double star system, then ejection of material from an accretion disc giving rise to hydrogen-deficient material could be the mechanism behind the observed abundance discrepancies.

A better understanding of the nature and origin of the H-deficient regions would result from much deeper and higher resolution spectra than have been analysed here, but it may be that the knots are so small that they will never be resolved.

ACKNOWLEDGMENTS

RW acknowledges support from a UK Particle Physics and Astronomy Research Council (PPARC) studentship. We thank the anonymous referee for a very thorough and useful report. MIDAS is developed and distributed by the ESO. IRAF is distributed by the National Optical Astronomy Observatories, which are operated by the Association of Universities for Research in Astronomy, Inc., under cooperative agreement with the National Science Foundation.

REFERENCES

Acker A., Ochsenbein F., Stenholm B., Tylenda R., Marcout J., Schohn C., 1992, Strasbourg–ESO Catalogue of Galactic Planetary Nebulae. Strasbourg, Obs. Strasbourg
Aggarwal K. M., 1983, ApJS, 52, 387
Allende Prieto C., Lambert D. L., 2001, ApJ, 556, 63
Allende Prieto C., Lambert D. L., Asplund M., 2002, ApJ, 573, L137
Aller L. H., Czyzak S. J., 1983, ApJS, 51, 211
Aller L. H., Keyes C. D., 1987, ApJS, 65, 405
Barker T., 1978, ApJ, 219, 914
Barker T., 1982, ApJ, 253, 167
Blum R., Pradhan A. K., 1992, ApJS, 80, 425
Brocklehurst M., 1972, MNRAS, 157, 211
Butler K., Zeippen C. J., 1989, A&A, 208, 337
Cahn J. H., Kaler J. B., Stanghellini L., 1992, A&AS, 94, 399
Clegg R. E. S., Peimbert M., Torres-Peimbert S., 1987, MNRAS, 224, 761
Cuisinier F., Acker A., Köppen J., 1996, A&A, 307, 215
Davey A. R., Storey P. J., Kisielius R., 2000, A&AS, 42, 85
De Marco O., Bond H. E., Harmer D., Fleming A. J., 2004, ApJ, 602, L93
Ercolano B., Barlow M. J., Storey P. J., Liu X-W., Rauch T., Werner K., 2003, MNRAS, 344, 1145
Ercolano B., Wesson R., Zhang Y., Barlow M. J., De Marco O., Rauch T., Liu X-W., 2004, MNRAS, 354, 558
Escalante V., Victor G. A., 1990, ApJS, 73, 513
Feibelman W. A., Hyung S., Aller L. H., 1996, MNRAS, 278, 625
Ferland G. J., 1992, ApJ, 389, 63
Fleming J., Bell K. L., Hibbert A., Vaeck N., Godefroid M. R., 1996, MNRAS, 279, 1289
French H. B., 1981, ApJ, 246, 434
Grevesse N., Sauval A. J., 1998, Space Sci. Rev., 85, 161
Henry R. B. C., 1990, ApJ, 356, 229
Henry R. B. C., Kwitter K. B., Howard J. W., 1996, ApJ, 458, 215
Howarth I. D., 1983, MNRAS, 203, 301
Hyung S., Aller L. H., Feibelman W. A., Lee W. B., 2001a, ApJ, 122, 954
Hyung S., Aller L. H., Lee W. B., 2001b, PASP, 113, 1159
Iben I., Kaler J. B., Truran J. W., 1983, ApJ, 264, 605
Johnson C. T., Kingston A. E., 1990, J. Phys. B, 23, 3393
Kaler J. B., 1970, ApJ, 160, 887
Kaler J. B., 1980, ApJ, 239, 78
Kaler J. B., Pratap P., Kwitter K. B., 1987, PASP, 99, 952
Keenan F. P., Feibelman W. A., Berrington K. A., 1992, ApJ, 389, 443
Keenan F. P., Hibbert A., Ojha P. C., Conlon E. S., 1993, Phys. Scr., 48, 129
Keenan F. P., Aller L. H., Bell K. L., Hyung S., McKenna F. C., Ramsbottom C. A., 1996, MNRAS, 281, 1073
King D. L., 1985, La Palma Technical Note 31
Kingdon J., Ferland G. J., 1995, ApJ, 442, 714
Kingsburgh R. L., Barlow M. J., 1994, MNRAS, 271, 257
Kisielius R., Storey P. J., Davey A. R., Neale L. T., 1998, A&AS, 133, 257
Kohoutek L., 1968, BAC, 19, 371
Kwitter K. B., Henry R. B. C., 1998, ApJ, 247, 259
Kwitter K. B., Henry R. B. C., 2001, ApJ, 562, 804
Lee P., Aller L. H., Kaler J. B., Czyzak S. J., 1974, ApJ, 192, 159
Liu X-W., 2003, in Kwok S., Dopita M., Sutherland R., eds, IAU Symp. 209, Planetary Nebulae: Their Evolution and Role in the Universe. Astron. Soc. Pac., San Francisco, p. 339
Liu X-W., Danziger I. J., 1993, MNRAS, 263, 256
Liu X-W., Storey P. J., Barlow M. J., Clegg R. E. S., 1995, MNRAS, 272, 369
Liu X-W., Storey P. J., Barlow M. J., Danziger I. J., Cohen M., Bryce M., 2000, MNRAS, 312, 585
Liu X-W., Luo S.-G., Barlow M. J., Danziger I. J., Storey P. J., 2001, MNRAS, 327, 141
Lutz J., 1981, ApJ, 247, 144
Mendoza C., 1983, in Flower D. R., ed., Planetary Nebulae. Kluwer, Dordrecht, p. 143
Mendoza C., Zeippen C. J., 1982a, MNRAS, 198, 127
Mendoza C., Zeippen C. J., 1982b, MNRAS, 199, 1025
Mendoza C., Zeippen C. J., 1983, MNRAS, 202, 981
Nussbaumer H., Rusca C., 1979, A&A, 72, 129
Nussbaumer H., Storey P. J., 1981, A&A, 99, 177
Nussbaumer H., Storey P. J., 1984, A&AS, 56, 293
Peimbert M., 1967, ApJ, 150, 825
Peimbert M., 1971, Bol. Obs. Tonantzintla y Tacubaya, 6, 29
Peimbert M., Costero R., 1969, Bol. Obs. Tonantzintla y Tacubaya, 5, 3
Peimbert M., Sarmiento A., Fierro J., 1991, PASP, 103, 815

Peimbert M., Storey P. J., Torres-Peimbert S., 1993, ApJ, 414, 626
Peimbert A., Peimbert M., Luridiana V., 2002, ApJ, 565, 668
Peimbert M., Peimbert A., Ruiz M. T., Esteban C., 2004, ApJS, 150, 431
Péquignot D., Petitjean P., Boisson C., 1991, A&A, 251, 680
Péquignot D., Liu X-W., Barlow M. J., Storey P. J., Morisset C., 2003, in Kwok S., Dopita M., Sutherland R., eds, IAU Symp. 209 Planetary Nebulae: Their Evolution and Role in the Universe. Astron. Soc. Pac., San Francisco, p. 347
Pradhan A. K., 1976, MNRAS, 177, 31
Rubin R. H., 1986, ApJ, 309, 334
Rubin R. H., 1989, ApJ, 69, 897
Ruiz M. T., Peimbert A., Peimbert M., Esteban C., 2003, ApJ, 595, 247
Smits D., 1996, MNRAS, 278, 683
Stafford R. P., Bell K. L., Hibbert A., Wijesundera W. P., 1994, MNRAS, 268, 816
Storey P. J., 1994, MNRAS, 282, 999
Storey P. J., Hummer D. G., 1995, MNRAS, 272, 41
Torres-Peimbert S., Peimbert M., Peña M., 1990, A&A, 233, 540
Torres-Peimbert S., Dufour R. J., Peimbert M., Peña M., 1997, in Habing H. J., Lamers H. J. G. L. M., eds, Proc. IAU Symp. 180, Planetary Nebulae. Kluwer, Dordrecht, p. 281
Tsamis Y. G., 2002, PhD thesis, University of London
Tsamis Y. G., Barlow M. J., Liu X-W., Danziger I. J., Storey P. J., 2003, MNRAS, 338, 687
Tsamis Y. G., Barlow M. J., Liu X-W., Storey P. J., Danziger I. J., 2004, MNRAS, 353, 953
Tylenda R., Acker A., Stenholm B., Köppen J., 1992, A&AS, 95, 337
Viegas S. M., Clegg R. E. S., 1994, MNRAS, 271, 993
Wesson R., Liu X-W., Barlow M. J., 2003, MNRAS, 340, 253
Wesson R., Liu X-W., 2004, MNRAS, 351, 1026
Zeippen C. J., 1982, MNRAS, 198, 111
Zeippen C. J., Le Bourlot J., Butler K., 1987, A&A, 188, 251
Zhang Y., Liu X-W., 2002, MNRAS, 337, 499
Zhang Y., Liu X-W., 2003, A&A, 404, 545
Zhang Y., Liu X-W., Wesson R., Storey P. J., Liu Y., Danziger I. J., 2004, MNRAS, 351, 935

SUPPLEMENTARY MATERIAL

The following supplementary material is available for this article online:
Table A1. Optical line lists.

APPENDIX A: OPTICAL LINE LISTS

Table A1 contains the line lists derived from the INT data for the sample nebulae. The columns contain, from left to right, the observed wavelength, the measured flux normalized to $F(\mathrm{H}\beta) = 100$, the dereddened flux, ionic identification, multiplet number, lower term and upper term of the transition, and statistical weights of the lower and upper levels.

Table A1. Optical line lists for the sample nebulae. (This is only a sample of this table: the full version is available online as supplementary material.)

λ_{obs}	$F(\lambda)$	$I(\lambda)$	Ion	λ_0	Mult	Lower term	Upper term	g_1	g_2
				Cn 3–1 line list 3500–5000Å					
3614.41	0.252	0.339	He I	3613.64	V6	2s 1S	5p 1P*	1	3
3635.36	0.124	0.166	He I	3634.25	V28	2p 3P*	8d 3D	9	15
3666.71	0.150	0.199	H 27	3666.10	H27	2p+ 2P*	27d+ 2D	8	*
3668.42	0.183	0.243	H 26	3667.68	H26	2p+ 2P*	26d+ 2D	8	*
3670.28	0.222	0.295	H 25	3669.47	H25	2p+ 2P*	25d+ 2D	8	*
3672.35	0.286	0.380	H 24	3671.48	H24	2p+ 2P*	24d+ 2D	8	*
3674.65	0.397	0.527	H 23	3673.74	H23	2p+ 2P*	23d+ 2D	8	*
3677.26	0.497	0.659	H 22	3676.36	H22	2p+ 2P*	22d+ 2D	8	*
3680.23	0.609	0.807	H 21	3679.36	H21	2p+ 2P*	21d+ 2D	8	*
3683.68	0.759	1.005	H 20	3682.81	H20	2p+ 2P*	20d+ 2D	8	*
3687.73	0.874	1.157	H 19	3686.83	H19	2p+ 2P*	19d+ 2D	8	*
3692.42	1.025	1.355	H 18	3691.56	H18	2p+ 2P*	18d+ 2D	8	*
3698.01	1.114	1.471	H 17	3697.15	H17	2p+ 2P*	17d+ 2D	8	*
3704.86	1.313	1.731	H 16	3703.86	H16	2p+ 2P*	16d+ 2D	8	*
3712.82	1.270	1.671	H 15	3711.97	H15	2p+ 2P*	15d+ 2D	8	*
3722.90	2.734	3.590	H 14	3721.94	H14	2p+ 2P*	14d+ 2D	8	*
3726.92	88.69	116.4	[O II]	3726.03	F1	2p3 4S*	2p3 2D*	4	4
3729.67	43.88	57.54	[O II]	3728.82	F1	2p3 4S*	2p3 2D*	4	6
3735.21	2.008	2.629	H 13	3734.37	H13	2p+ 2P*	13d+ 2D	8	*
3751.01	2.249	2.935	H 12	3750.15	H12	2p+ 2P*	12d+ 2D	8	*
3771.49	2.985	3.878	H 11	3770.63	H11	2p+ 2P*	11d+ 2D	8	*
3798.75	3.639	4.700	H 10	3797.90	H10	2p+ 2P*	10d+ 2D	8	*
3820.51	0.313	0.402	He I	3819.62	V22	2p 3P*	6d 3D	9	15
3836.21	4.725	6.052	H 9	3835.39	H9	2p+ 2P*	9d+ 2D	8	*
3856.65	0.064	0.082	O II	3856.13	V12	3p 4D*	3d 4D	4	2
3889.73	10.14	12.84	H 8	3889.05	H8	2p+ 2P*	8d+ 2D	8	*
	*	*	He I	3888.65	V2	2s 3S	3p 3P*	3	9
3919.72	0.056	0.070	C II	3918.98	V4	3p 2P*	4s 2S	2	2
3921.31	0.109	0.137	C II	3920.69	V4	3p 2P*	4s 2S	4	2
3934.03	−0.318	−0.399	Ca II	3933.66	V1	4s 2S	4p 2P*	2	4
3965.50	0.464	0.578	He I	3964.73	V5	2s 1S	4p 1P*	1	3
3970.83	11.72	14.58	H 7	3970.07	H7	2p+ 2P*	7d+ 2D	8	98

APPENDIX B: ULTRAVIOLET AND INFRARED LINE LISTS

Table B1. Infrared line fluxes for the nebulae observed with the *ISO* satellite. $F(\lambda)$ is in units of 10^{-13} erg cm^{-2} s^{-1}, $I(\lambda)$ is normalized to $I(\mathrm{H}\beta) = 100$ using Hβ fluxes from Cahn et al. (1992). Critical densities are taken from Rubin (1989).

Nebula		Hu 2–1	Me 2–2	NGC 6891	Vy 2–2
H I Br α 4.05 µm	$F(\lambda)$	3.669	0.901	*	*
	$I(\lambda)$	3.867	5.912	*	*
H I Pf β 4.65 µm	$F(\lambda)$	7.518	*	*	*
	$I(\lambda)$	7.924	*	*	*
[Ar III] 8.99 µm	$F(\lambda)$	4.180	*	8.386	6.086
($n_{\mathrm{crit}} = 2.75 \times 10^5$ cm^{-3})	$I(\lambda)$	4.406	*	19.79	4.911
[S IV] 10.51 µm	$F(\lambda)$	*	*	10.32	*
($n_{\mathrm{crit}} = 4.99 \times 10^4$ cm^{-3})	$I(\lambda)$	*	*	24.36	*
[Ne II] 12.81 µm	$F(\lambda)$	8.575	*	*	13.21
($n_{\mathrm{crit}} = 5.91 \times 10^5$ cm^{-3})	$I(\lambda)$	9.038	*	*	10.66
[Ne III] 15.56 µm	$F(\lambda)$	13.79	10.95	42.19	17.90
($n_{\mathrm{crit}} = 1.27 \times 10^5$ cm^{-3})	$I(\lambda)$	14.54	71.85	99.57	14.45
[S III] 18.71 µm	$F(\lambda)$	2.117	*	1.955	*
($n_{\mathrm{crit}} = 1.40 \times 10^4$ cm^{-3})	$I(\lambda)$	2.231	*	4.614	*
[S III] 33.49 µm	$F(\lambda)$	*	*	3.999	*
($n_{\mathrm{crit}} = 1.78 \times 10^3$ cm^{-3})	$I(\lambda)$	*	*	9.438	*

Table B2. Ultraviolet line fluxes for the nebulae observed with *IUE* SWS, normalized to $F(\mathrm{H}\beta) = 100$ using Hβ fluxes from Cahn et al. (1992).

Nebula	C IV λ1550		He II λ1640		O III] λ1663		N III] λ1751		C III] λ1909	
	$F(\lambda)$	$I(\lambda)$	$F(\lambda)$	$I(\lambda)$	$F(\lambda)$	$I(\lambda)$	$F(\lambda)$	$I(\lambda)$	$F(\lambda)$	$I(\lambda)$
DdDm 1	*	*	*	*	*	*	*	*	7.110	10.49
Hu 2–1	*	*	*	*	*	*	*	*	12.31	112.2
IC 1747	9.311	143.3	23.83	325.3	*	*	0.847	11.14	36.96	635.0
IC 2003	116.3	300.3	128.2	317.6	8.111	19.94	7.818	19.11	132.7	356.0
IC 351	66.36	189.5	67.89	185.2	8.014	21.69	*	*	83.61	249.2
IC 4846	7.338	49.44	*	*	*	*	*	*	6.001	43.68
IC 5217	13.39	52.66	14.91	55.23	5.498	20.15	2.585	9.401	30.00	124.7
M 3–27	*	*	*	*	23.98	304.3	10.82	135.1	81.47	1322
NGC 6803	*	*	2.260	21.90	*	*	1.155	10.84	4.312	51.05
NGC 6833	*	*	*	*	*	*	*	*	30.17	30.17
NGC 6891	*	*	*	*	*	*	*	*	20.10	45.47
NGC 7026	4.938	104.0	4.602	84.81	*	*	*	*	1.899	45.23
Vy 1–2	4.073	5.955	69.23	99.55	5.185	7.435	6.686	9.567	36.70	54.50

Table B3. Ultraviolet line fluxes for the nebulae observed with *IUE* LWS, normalized to $F(\mathrm{H}\beta) = 100$ using Hβ fluxes from Cahn et al. (1992).

Nebula		DdDm 1	Hu 2–1	IC 1747	IC 2003	IC 351	IC 4846	IC 5217	NGC 7026	Vy 1–2
C II λ2326	$F(\lambda)$	2.539	12.34	*	*	*	13.18	5.593	*	*
	$I(\lambda)$	3.888	141.6	*	*	*	118.0	26.98	*	*
Ne IV λ2423	$F(\lambda)$	*	*	*	17.28	14.52	*	3.086	*	16.47
	$I(\lambda)$	*	*	*	42.31	39.12	*	11.25	*	23.58
O II λ2470	$F(\lambda)$	3.343	8.072	*	*	*	*	*	*	3.205
	$I(\lambda)$	4.622	50.69	*	*	*	*	*	*	4.452
He II λ2733	$F(\lambda)$	*	*	0.830	6.182	2.869	*	*	*	4.819
	$I(\lambda)$	*	*	4.119	10.78	5.308	*	*	*	6.021
O III λ2837	$F(\lambda)$	*	*	*	4.586	3.382	1.960	1.457	*	6.618
	$I(\lambda)$	*	*	*	7.496	5.825	5.267	2.962	*	8.058
O III λ3132	$F(\lambda)$	*	*	7.228	40.55	40.32	*	9.392	4.700	37.67
	$I(\lambda)$	*	*	20.23	57.96	59.87	*	15.73	14.81	43.47
O III λ3047	$F(\lambda)$	*	*	*	*	*	*	*	0.726	7.331
	$I(\lambda)$	*	*	*	*	*	*	*	2.549	8.573

APPENDIX C: ATOMIC DATA REFERENCES

Table C1. Atomic data references.

ORLs Ion		Effective Recombination Coefficients
He I		Brocklehurst (1972)
C II		Davey, Storey & Kisielius (2000)
N II		Escalante & Victor (1990)
N III		Péquignot et al. (1991)
Ne II		Kisielius et al. (1998)
O II		Storey (1994)
O III		Péquignot et al. (1991)
CELs Ion	Transition Probabilities	Collision Strengths
Ar III	Mendoza & Zeippen (1983)	Johnson & Kingston (1990)
Ar IV	Mendoza & Zeippen (1982a)	Zeippen, Le Bourlot & Butler (1987)
C II	Nussbaumer & Storey (1981)	Blum & Pradhan (1992)
C III	Keenan, Feibelman & Berrington (1992), Fleming et al. (1996)	Keenan et al. (1992)
Cl III	Mendoza & Zeippen (1982b)	Butler & Zeippen (1989)
N II	Nussbaumer & Rusca (1979)	Stafford et al. (1994)
O II	Zeippen (1982)	Pradhan (1976)
O III	Nussbaumer & Storey (1981)	Aggarwal (1983)
S II	Mendoza & Zeippen (1982a), Keenan et al. (1993)	Keenan et al. (1996)
S III	Mendoza & Zeippen (1982b)	Mendoza (1983)

This paper has been typeset from a TEX/LATEX file prepared by the author.